Energy Economics 148 (2025) 108586

Contents lists available at ScienceDirect

Energy Economics

journal homepage: www.elsevier.com/locate/eneeco

Seasonality and spikes in the natural gas market

Francesco Rotondi

Department of Finance, Bocconi University, Milano, Italy

ARTICLE INFO

JEL classification:
G13
Q40
C60

Keywords:
Natural gas
Commodity prices
Stochastic convenience yield
Seasonality
Jumps

ABSTRACT

In this paper we propose and examine an arbitrage-free model for the natural gas spot price and its convenience yield. Performing an empirical analysis of the European natural gas spot and futures markets, we observe that log spot prices are non-stationary, exhibit mild seasonality, and display almost continuous behaviour. In contrast, the implied convenience yield is stationary, shows strong seasonality, and experiences frequent spikes. Motivated by this evidence, we model the spot convenience yield as a combination of a deterministic seasonal component and a mean-reverting stochastic process with jumps. By assuming an appropriate distribution for the jump component, we derive a closed-form expression for futures prices. Our model demonstrates an excellent fit to European data, both before and after the COVID-19 pandemic and the Russia–Ukraine war.

1. Introduction

Among commodities, natural gas[1] is particularly important due to its versatility, efficiency and comparatively lower environmental impact as opposed to other fossil fuels. Indeed, natural gas serves as a crucial energy source for heating, electricity generation, industrial processes and also as a critical backup for renewable energy sources, ensuring energy stability and reliability.

As a result, the annual consumption of natural gas has been steadily increasing. For instance,[2] in the United States, natural gas consumption rose from 23 trillion cubic feet in 2020 to nearly 33 trillion in 2023. At the same time, natural gas financial markets have gained increasing importance, evidenced by a sharp rise in the trading volume of natural gas futures contracts and the introduction of various derivatives based on them. As an illustrative example,[3] the trading volume of natural gas futures contracts at Intercontinental Exchange, Inc. (ICE), one of the largest American companies serving as a clearing house for commodity futures, has increased from 523,365 traded futures contracts on natural gas in 2000 to 64,766,711 in 2023.

Natural gas futures markets exhibit pronounced seasonality and sudden price spikes. While these characteristics could be incorporated directly into the spot price dynamics, thereby influencing futures prices, standard no-arbitrage restrictions in commodity pricing applications impose that the expected growth rate of the spot price must be equal to the risk-free rate minus the convenience yield.

To ensure consistency with this constraint and building upon the foundational work of Gibson and Schwartz (1990), this paper introduces a model that integrates both seasonality and discontinuities within a stochastic convenience yield process rather than within the spot price. This formulation preserves the no-arbitrage condition while effectively capturing the distinctive features of the natural gas futures market.

More precisely, we model the spot convenience yield as comprising two components: a deterministic seasonal factor, represented by a periodic function of time, and a mean-reverting jump-diffusive stochastic process.[4] This framework successfully captures three key empirical features of the European natural gas market:

1. the non-stationarity of the log spot price and the stationarity of its spot convenience yield;
2. frequent spikes in the spot convenience yield, in contrast to the nearly continuous behaviour of the log spot price;
3. strong seasonality in the spot convenience yield, with much weaker seasonality in the log spot price.

Using tools from stochastic calculus for jump-diffusive processes, we derive the Laplace transform of the relevant variables and, assuming

E-mail address: rotondi.francesco@unibocconi.it.

[1] See Chapter 3 of Roncoroni et al. (2015) for an effective introduction to natural gas physical characteristics and for a detailed overview of the main natural gas financial markets and products.

[2] See here.

[3] See here.

[4] Our approach is akin to the model proposed by Das (2002) for the short-term interest rate and belongs to the class of affine jump–diffusion models analysed in Duffie et al. (2000), initially introduced in Merton (1976).

https://doi.org/10.1016/j.eneco.2025.108586
Received 7 June 2024; Received in revised form 30 April 2025; Accepted 10 May 2025
Available online 29 May 2025

a suitable distribution for the jump component, obtain closed-form solutions for natural gas futures prices. A maximum likelihood-based estimation and further numerical experiments confirm that our model effectively replicates both the observed spot price dynamics and the convenience yield characteristics. Moreover, the inclusion of jumps in the convenience yield enables the model to capture the irregular forward curves that emerged in the European natural gas market following the COVID-19 pandemic and the Russia–Ukraine war.

Our empirical findings demonstrate a strong fit between the model and observed forward curves, both before and after these disruptive events, highlighting the relevance of the seasonal and jump components in capturing usual and unusual market conditions.

As already mentioned, the assumption of a constant convenience yield was first challenged by Gibson and Schwartz (1990), who introduced a two-factor model in which the convenience yield follows a mean-reverting stochastic process. Subsequent extensions include (Miltersen, 2003), who modified the model to achieve a perfect fit of the observed forward curve, and Casassus and Collin-Dufresne (2005), who introduced a three-factor model incorporating interest rate dependency. More recently, Almansour (2016) introduced regime-dependent parameters for natural gas, and Li (2019) proposed a discrete-time model incorporating GARCH and jump features.

All of these works and most of the existing literature adopts a "spot convenience yield modelling" approach, which enables closed-form solutions for futures and option pricing but struggles to precisely fit observed forward curves, as noted in Carmona and Ludkovski (2004). An alternative approach, "convenience yield term structure modelling", builds on the Heath–Jarrow–Morton framework and has been applied to energy markets by Miltersen and Schwartz (1998) and Björk and Landen (2000), and more recently by Benth et al. (2019).

Seasonality in commodities was first emphasized by Schwartz and Smith (2000) and Lucia and Schwartz (2002), with García Mirantes et al. (2013) proposing a fully stochastic four-factor model to account for both short- and long-term seasonal effects. The importance of jumps in commodity prices has been recognized since Hilliard and Reis (1999) and further explored by Kyriakou et al. (2016) and Nguyen and Prokopczuk (2019). More recently, Callegaro et al. (2022) used branching processes and Hawkes processes to replicate clustered jumps in forward prices.

Our model contributes to this literature by explicitly modelling both seasonality and jumps within the stochastic convenience yield process, offering a flexible yet tractable framework for capturing the unique features of natural gas markets while satisfying the standard no-arbitrage restrictions of risk-neutral market models.

The paper is organized as follows. Section 2 provides an overview of the European natural gas spot and futures markets. It describes the dataset, displays a few forward curves, and analyzes the properties of the time series for the natural gas spot price and the implied convenience yield. Section 3 addresses the jump-diffusive stochastic model for the natural gas spot price and its convenience yield. It presents the stochastic differential equations governing the variables of interest, their solutions, the closed-form solution for futures prices, how to deal with the pricing of non-linear payoffs, a numerical simulation of the model and a final extension of the benchmark model to incorporate a jump component also in the spot price process. In Section 4, we apply our model to the data and examine its fit to the observed forward curves. Section 5 concludes the paper. The Appendix contains the proofs of the results in the main text along with some ancillary technical details.

2. The european natural gas market

This section contains an overview of the European natural gas spot and futures markets. In particular, Section 2.1 features the description of the dataset and a few preliminary plots of the series of interest while Section 2.2 contains the analysis of the empirical characteristics of the time series of the natural gas log spot price and of the implied convenience yield.

2.1. Overview of the spot and futures market

As already stated in the previous section, we target our analysis to the European natural gas market. Trading of natural gas contracts takes place on various hubs, with the Dutch Title Transfer Facility (TTF) being one of the most prominent. Natural gas futures traded at the TTF[5] include daily futures, which are used to balance short-term demand and supply, and monthly futures, with maturities ranging from one month to ten years; among these, the most liquid contracts are those with maturities of less than two years. Following the standard approach, we use the day t-price of the one-day ahead futures contract as a proxy for the natural gas spot price S_t.

For our empirical analysis we consider daily settlement prices, quoted in Euro per megawatt hour, of the one-day ahead futures and of all the available monthly futures starting from March 15, 2010 to February 29, 2024, for a total of 3'644 trading days and 282'439 observations.[6]

At each observation date t, the monthly futures prices with different maturities $\{T_i\}_i$ form the so-called natural gas forward curve, $\{F(t,T_i)\}_i$. The collection of the forward curves with maturities up to forty-eight months delivers the natural gas forward surface depicted in Fig. 1.

Since 2010, European natural gas prices have experienced significant fluctuations driven by various macro-economic factors. Recently, the COVID-19 pandemic caused an initial price drop in 2020, followed by a surge in 2021 due to supply chain issues and economic recovery. Record highs were reached in 2022 due to the Russia–Ukraine conflict and resulting supply disruptions. As shown in the top panel of Fig. 1, spot and futures prices during this period significantly surpass those of previous years.

On top of the significant differences in the levels of both spot and futures prices, the latter also exhibit varying behaviours when normalized to the current spot price and analysed day by day. Fig. 2 displays the normalized forward curves, defined as $\{F(t,T_i)/S_t\}_i$ on the first trading day of each year in the sample. In the left panel of Fig. 2, it is evident that prior to 2020, the forward curves predominantly hovered around one (i.e. around their spot price), displaying notable seasonality with a twelve-month cycle attributable to the annual demand and supply patterns. However, examining the right panel of Fig. 2, we observe significant departures from this typical behaviour in forward curves. Despite some lingering seasonality, the curves no longer centre around one; instead, they demonstrate shifts that consistently impact their long-term mean level.

Given that these anomalies observed in futures prices cannot solely be attributed to disruptions in the spot market, we now turn to an empirical analysis of the implied convenience yield.

2.2. Stylized facts of the spot price and of the implied convenience yield

In commodity price modelling, the concept of convenience yield encapsulates the benefit or drawback associated with holding physical inventories of the commodity rather than a financial contract representing ownership of that commodity. Initially introduced as the price of storage by Nicholas (1939) and usually labelled by δ, the convenience yield denotes the (potentially stochastic) net flow of these advantages or disadvantages per unit of time and commodity.

Assuming the independence of the spot price S from both the risk-free interest rate r and the convenience yield δ, according to the

[5] The specifics of daily futures are available here while the specifics of monthly contracts are available here.

[6] Prices are obtained from Datastream using mnemonic TRNLTTD for the one-day ahead futures and mnemonics ETMmmyy for the monthly futures for delivery at the beginning of month mm, year yy.

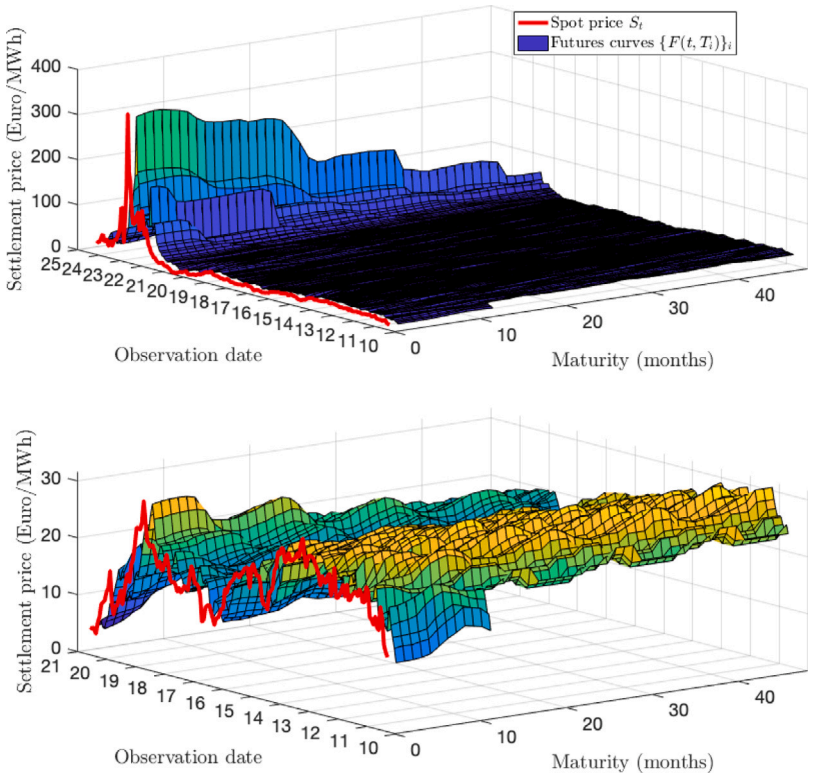

Fig. 1. Top panel: natural gas spot price and forward surface from 2010 to 2024; bottom panel: zoom-in of the top panel over the 2010–2020 period.

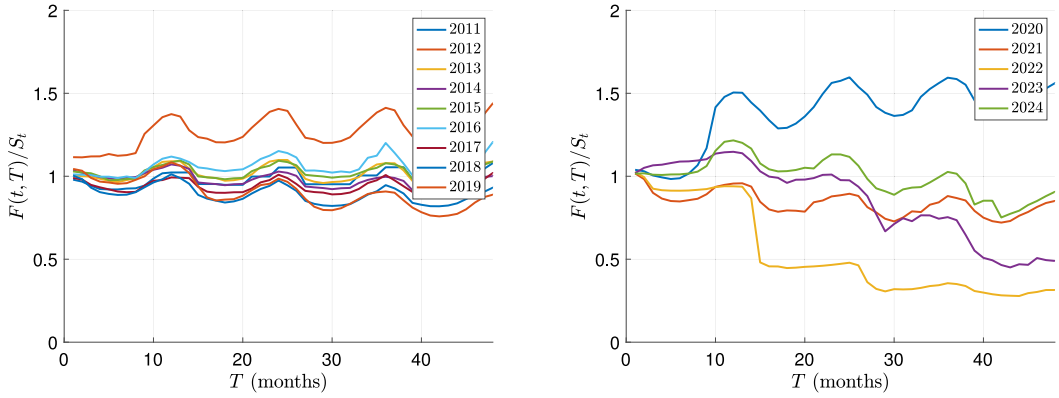

Fig. 2. Normalized forward curves on the first trading day of the year.

standard no-arbitrage theory[7] the time-t price $F(t,T)$ of a forward contract on S with maturity T is equal to

$$F(t,T) = S_t \mathbb{E}\left[\exp\left(\int_t^T \left(r(s) - \delta_s\right) \mathrm{d}s\right)\right], \tag{1}$$

where the expected value is taken under an equivalent martingale measure. The challenge here lies in the unobservability of the convenience yield.

Given that stochastic models are formulated on the instantaneous convenience yield δ_t, it becomes imperative to identify a proxy for it that can be empirically computed. One way to go, is to focus at time t on the futures price with the closest maturity t^+, set both $r(s)$ and δ_s in (1) constantly equal to $r(t)$ and δ_t between t and t^+ and, finally, solve for δ_t. Doing so, we can explicitly compute a proxy $\hat{\delta}_t$ for the instantaneous convenience yield as[8]

$$\hat{\delta}_t = r(t) - \frac{1}{t^+ - t} \ln \frac{F(t,t^+)}{S_t}. \tag{2}$$

Notice that in practice,[9] the time to maturity, $t^+ - t$, varies from one day to thirty days, depending on the positioning of t within the month.

Since our final goal is to specify a stochastic model for both the (log) spot price and the convenience yield, we describe now some insightful stylized facts of the two main series of interest in levels and

[7] See, e.g., the first section of Carmona and Ludkovski (2004).

[8] Notice that this formula corresponds to the one used in Gibson and Schwartz (1990) to retrieve the convenience yield from crude oil futures prices.

[9] The short-term risk-free interest rate $r(t)$ in (2) is computed according to the methodology of Svensson (1994). Specifically, it is assumed that $r(t) = \beta_0 + \beta_1 \exp\left(-t/\tau_1\right) + \beta_2 \frac{t}{\tau_1} \exp\left(-t/\tau_1\right) + \beta_3 \frac{t}{\tau_2} \exp\left(-t/\tau_2\right)$. The daily estimates of the parameters $(\beta_0, \beta_1, \beta_2, \beta_3, \tau_1, \tau_2)$ are provided by the European Central Bank here and are derived from the prices of Euro-denominated AAA-rated government bonds.

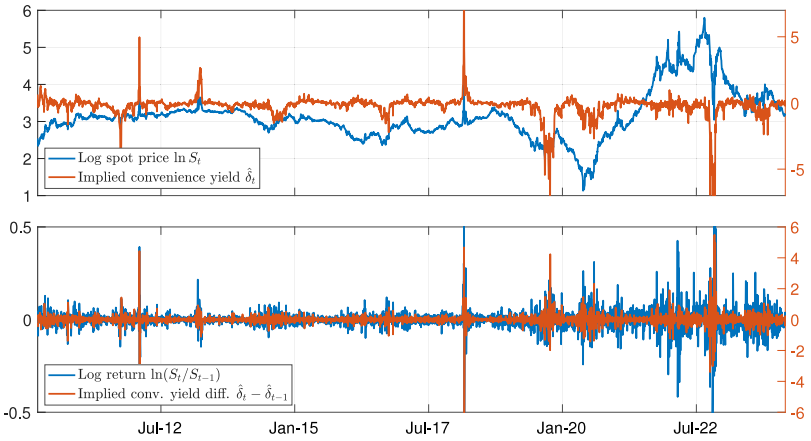

Fig. 3. Natural gas log spot price (left axis) and implied convenience yield (right axis) according to (2) in levels (top panel) and first differences (bottom panel).

Table 1
P-values of the ADF and of the KPSS tests for the four series of interest.

test	$\ln S_t$	$\ln(S_t/S_{t-1})$	$\hat{\delta}_t$	$\hat{\delta}_t - \hat{\delta}_{t-1}$
ADF	0.5206	≤ 0.001	≤ 0.001	≤ 0.001
KPSS	≤ 0.01	≥ 0.1	≤ 0.01	≥ 0.1

Table 2
Sample centred moments of the four series of interests.

	$\ln S_t$	$\ln(S_t/S_{t-1})$	$\hat{\delta}_t$	$\hat{\delta}_t - \hat{\delta}_{t-1}$
Mean	3.13873	0.00018	−0.23321	−0.00016
Variance	0.41973	0.00322	0.85047	0.14889
Skewness	1.02082	−0.12327	−4.45811	−0.27082
Kurtosis	5.35704	51.23496	72.15817	121.73717

in first differences. In particular, we consider: the log spot price series $\{\ln S_t\}_t$, its first differences, $\{\ln S_t - \ln S_{t-1}\}_t$, namely the log return series $\{\ln S_t/S_{t-1}\}_t$, the convenience yield series $\{\hat{\delta}_t\}_t$ as defined in (2) and its first differences, $\{\hat{\delta}_t - \hat{\delta}_{t-1}\}_t$.

Fig. 3 displays these four series. Looking at these plots, we can list three relevant features of the processes under analysis that will guide our modelling choices:

1. the log spot price seems to contain a unit root as the series of the levels does not look stationary while the one of the first differences does; on the contrary, the series of the levels of the implied convenience yield seems stationary already and not very persistent, as the shocks hitting the series are quickly absorbed; as it can be seen in Table 1, these qualitative assessments are confirmed by the augmented Dickey–Fuller (ADF, Said and Dickey (1984)) test for the presence of a unit root and by the Kwiatkowski–Phillips–Schmidt–Shin (KPSS, Kwiatkowski et al. (1992)) test for the stationarity of the series, but for the KPSS test on $\hat{\delta}_t$. In this case, the statistical rejection of stationarity could be due to the presence of a deterministic period trend, as discussed below;
2. the convenience yield series in levels exhibits frequent and substantial spikes, while the log price series in levels shows a nearly continuous behaviour. This observation aligns with the sample centred moments reported in Table 2. Specifically, the convenience yield and its first differences show the largest deviations in skewness and kurtosis from the Gaussian benchmarks;
3. the convenience yield series in levels exhibits the strongest seasonality. Fig. 4 shows the dominant seasonal component obtained through the non-parametric singular spectrum analysis (SSA) detailed in Chapter 2 of Golyandina and Zhigljavsky (2013). As illustrated, a clear seasonal pattern is detectable only in the levels of the convenience yield series, while it is much weaker in the other three series.

Guided by these three stylized facts, in the following section we propose a model for the natural gas market that extends the two-factor model originally proposed by Gibson and Schwartz (1990) (GS model, henceforth) for the crude oil market. Consistently with the first stylized fact (stationarity of log returns and the levels of the convenience yield), the model assumes a conditionally log-normal spot price process and a stationary convenience yield. Moreover, in order to incorporate the other two stylized facts (seasonality and spikes in its levels) that were not accounted for in the original GS model, we model the stochastic convenience yield process as the sum of a seasonal component and an Ornstein–Uhlenbeck process that exhibits also idiosyncratic jumps.

Before turning to the formal description of the model it is worthy to mention that energy-linked commodities in general exhibit some degree of seasonality and occasional price spikes. In the Supplementary Materials, we present a comparative analysis of the European crude oil and coal markets, replicating a subset of the analyses carried out on natural gas to highlight their distinct dynamics. Our findings show that, in these markets, the GS model performs reasonably well without requiring any extensions.

3. The jump-diffusive stochastic convenience yield model

This section deals with our model for the natural gas spot price and its convenience yield. In particular, we introduce the stochastic differential equations driving the two in Section 3.1 and we solve them in Section 3.2. Afterwards, in Section 3.3 we derive the Laplace transform of the variables of interest in order to obtain a closed form expression for futures prices. In Section 3.4 we show how to deal with the pricing on non-linear payoffs while in Section 3.5 we simulate the model in order to verify whether it can reproduce the stylized empirical features described in the previous section. Finally, in Section 3.6 we present an extension of the model featuring a jump component also within the spot price process.

3.1. Dynamics of the model

Consider a frictionless arbitrage-free financial market modelled by a filtered probability space $(\Omega, \mathcal{F}, \mathbb{F} = (\mathcal{F}_t)_{t\geq 0}, \mathbb{Q})$ supporting all the variables introduced in the following and where $\mathbb{Q}$ is an equivalent martingale measure. Moreover, assume a deterministic term structure, with $r(t)$ representing the spot rate interest rate. As in Section 2.2, $r(t)$ is modelled using the deterministic functional form proposed by Svensson (1994), recalled in footnote 9. Let $S = (S_t)_{t\geq 0}$ represent the spot price of natural gas and $B = (B_t)_{t\geq 0}$ the price process of the money market

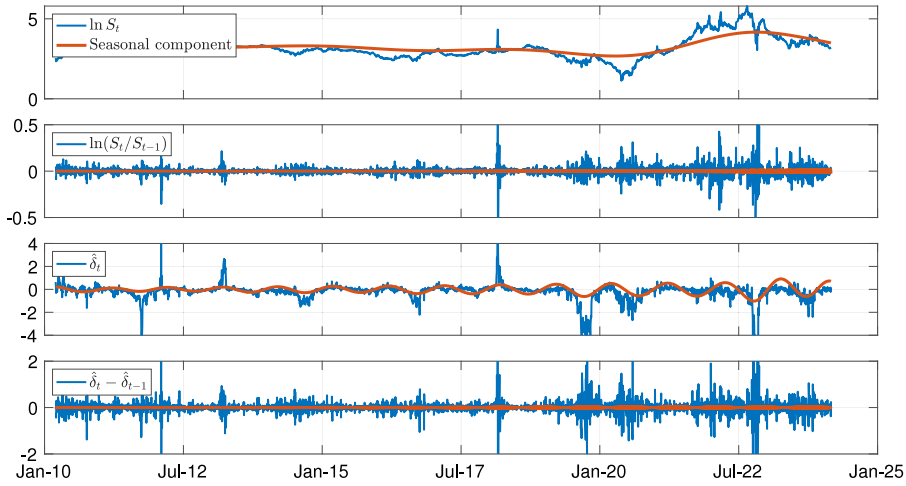

Fig. 4. Prevailing seasonal components obtained by SSA of the four series of log spot prices (in levels and in first differences, i.e. log returns) and of the implied convenience yield (in levels and in first differences).

account defined as $B_t = \exp\left(\int_0^t r(s)\mathrm{d}s\right)$. Finally, let $\delta = (\delta_t)_{t\geq 0}$ represent the stochastic convenience yield of S.

To incorporate the stylized features of the natural gas spot and futures markets discussed in the previous section we choose to include both the seasonal and jump components in the convenience yield process δ. More precisely, we assume that this process features two components: a deterministic seasonal term, represented by a periodic function $g(t)$, and a jumping Ornstein–Uhlenbeck (JOU) process $x = (x_t)_{t\geq 0}$, which is a mean-reverting process with jumps. In this way, the seasonal component remains persistent while any jump that might occur is eventually absorbed thanks to the mean-reversion property of the second component of δ.

Formally, the market model is described by the following equations

$$\frac{\mathrm{d}S_t}{S_t} = \left(r(t) - \delta_t\right)\mathrm{d}t + \sigma_S \mathrm{d}W_t^S \tag{3}$$

$$\mathrm{d}\delta_t = g'(t)\mathrm{d}t + \mathrm{d}x_t \tag{4}$$

$$\mathrm{d}x_t = \kappa\left(\theta - x_{t^-}\right)\mathrm{d}t + \sigma_x \mathrm{d}W_t^x + \mathrm{d}J_t \tag{5}$$

with initial conditions $S_0 \in \mathbb{R}^+$, $x_0 \in \mathbb{R}$ and $\delta_0 = g(0) + x_0$ and where

- $W^S = (W_t^S)_{t\geq 0}$ and $W^x = (W_t^x)_{t\geq 0}$ are two standard Brownian motions with correlation $\rho \in [-1, 1]$ representing respectively the sources of market risk and convenience yield risk;
- $g(t) : \mathbb{R}^+ \to \mathbb{R}$ is a periodic function capturing seasonality. Following the pioneer work of Harvey (1989) in the modelling of seasonal time series, we assume

  $$g(t) = a\cos(bt + c) \tag{6}$$

  with $a, b, c, \in \mathbb{R}$, that, when integrated, creates a sine wave;
- $J = (J_t)_{t\geq 0}$, with $J_t = \sum_{j=1}^{N_t} Y_j$, is a compound Poisson process with intensity $\lambda \in \mathbb{R}^+$ and where the Y_j's are i.i.d. random variables representing jumps with probability density function (resp. cumulative distribution function) $f_Y(y)$ (resp. $F_Y(y)$) and support $supp(Y)$. $N = (N_t)_{t\geq 0}$ is a counting process with random arrival/jumping times τ_j's.[10] Y_j's and τ_j's are assumed to be independent of each other and, moreover, they are assumed to be independent of W^S and W^x;
- $x_{t^-} := \lim_{u\uparrow t} x_u$ (and $x_t = \lim_{u\downarrow t} x_u$) represents the value of process x at time t right before a potential jump. If the jth jump arrives at time t (i.e. if $\tau_j = t$) we have

  $$x_t = x_{t^-} + Y_j \tag{7}$$

  while, if there is no jump at time t, we simply have $x_t = x_{t^-}$;
- $\sigma_S, \sigma_x \in \mathbb{R}^+$ represent respectively the volatility of the spot price and of the convenience yield while $\kappa, \theta \in \mathbb{R}$ represent respectively the speed of mean-reversion and the long run mean of the latter.

The last thing we need to specify at this point is the precise distribution of the jumps Y_j's. As the plain Ornstein–Uhlenbeck process alone is normally distributed, a natural choice would be to assume normally distributed jumps. However, as we will point out, this choice does not allow for an explicit closed form solution for futures prices. Therefore, for sake of tractability, we assume that the jumps follow a centred double exponential distribution (also known as the Laplace distribution[11]), namely

$$f_Y(y) = \frac{\phi}{2}\exp(-\phi|y|) = \frac{\phi}{2}\left(\exp(\phi y)\mathbf{1}_{\{y\leq 0\}} + \exp(-\phi y)\mathbf{1}_{\{y>0\}}\right) \tag{8}$$

with $\phi \in \mathbb{R}^+$ and where $\mathbf{1}_{\{A\}}$ is the indicator function of event A. It holds $\mathbb{E}[Y] = 0$ and $V[Y] = \frac{2}{\phi^2}$.

Remark 1. The model we just described encapsulates the original GS model as a specific case when there is neither seasonality, namely when $g(\cdot) \equiv 0$, nor a jump component, namely when $\lambda = 0$.

Remark 2. As the primary focus of this study is on futures pricing, the proposed model is formulated directly under a risk-neutral measure $\mathbb{Q}$. However, this martingale-based approach does not explicitly account for risk premia, which can be identified by also analysing the model's dynamics under the physical measure $\mathbb{P}$. This analysis is presented in Appendix A of Appendix.

3.2. Solutions of the model

We now look for the (conditional) solutions of the processes defined through (3)–(5).

Itô's formula applied to $\log S_t$ delivers

$$\mathrm{d}\log S_t = \left(r(t) - \delta_t - \frac{\sigma_S^2}{2}\right)\mathrm{d}t + \sigma_S \mathrm{d}W_t^S.$$

Integrating $\mathrm{d}\log S_t$ from u to t and taking the exponential of the result yields

$$S_t = S_u \exp\left(\int_u^t \left(r(s) - \delta_s\right)\mathrm{d}s - \frac{\sigma_S^2}{2}(t-u) + \sigma_S\left(W_t^S - W_u^S\right)\right). \tag{9}$$

[10] It holds $N_t \sim Poisson(\lambda t)$ and $\tau_{j+1} - \tau_j \sim Exponential(\lambda t)$ for all $j \in \mathbb{N}$.

[11] This was also the choice of Kou and Wang (2004) for the jumps hitting the price of an equity price process.

As far as the total convenience yield process in (4) is concerned, we simply get

$$\delta_t = g(t) + x_t. \tag{10}$$

The solution of the JOU process x requires the application of the Itô's formula for jump-diffusive processes.[12] If $\mathrm{d}x_t^c := \kappa\left(\theta - x_t\right)\mathrm{d}t + \sigma_x \mathrm{d}W_t^x$ represents the continuous part of $\mathrm{d}x_t$ in (5), applying Itô's formula to $x_t e^{\kappa t}$ delivers

$$\begin{aligned}\mathrm{d}x_t e^{\kappa t} &= \kappa x_{t^-} e^{\kappa t}\mathrm{d}t + e^{\kappa t}\mathrm{d}x_t^c + \left(x_t e^{\kappa t} - x_{t^-} e^{\kappa t}\right)\left(N_t - N_{t^-}\right)\\ &= e^{\kappa t}\left(\kappa\theta \mathrm{d}t + \sigma_x \mathrm{d}W_t^x + \left(x_t - x_{t^-}\right)\left(N_t - N_{t^-}\right)\right).\end{aligned}$$

Integrating between u and t we get

$$x_t e^{\kappa t} = x_u e^{\kappa u} + \theta\left(e^{\kappa t} - e^{\kappa u}\right) + \sigma_x \int_u^t e^{\kappa s}\mathrm{d}W_s^x + \sum_{j=N_u}^{N_t} e^{\kappa\tau_j}\left(x_{\tau_j} - x_{\tau_j^-}\right).$$

Using (7) for the jump component and rearranging the terms from the previous expression we get

$$x_t = x_u e^{-\kappa(t-u)} + \theta\left(1 - e^{-\kappa(t-u)}\right) + \sigma_x \int_u^t e^{-\kappa(t-s)}\mathrm{d}W_s^x + \sum_{j=N_u}^{N_t} e^{-\kappa\left(t-\tau_j\right)} Y_j. \tag{11}$$

Interestingly, this process remains mean-reverting since each jump Y_j is absorbed and forgotten thanks to the discount factor $e^{-\kappa(t-\tau_j)}$ and the long-run mean of x is still equal to θ.

Remark 3. While the stochastic integral in (11) is normally distributed, the distribution of x_t clearly depends on the distribution of the i.i.d. jumps. However, even assuming normally distributed jumps, each jump is weighted by a discount factor that involves a random time and, therefore, their sum is no longer normally distributed.

3.3. Futures pricing

If there is no interest rate risk, the time-t price of a futures contract on S with maturity T can be computed as $F(t,T) = \mathbb{E}\left[S_T \middle| \mathcal{F}_t\right]$. Combining (9) with (10) we get

$$F(t,T) = \mathbb{E}\left[S_t \exp\left(\int_t^T \left(r(s) - \left(g(s) + x_s\right)\right)\mathrm{d}s - \frac{\sigma_S^2}{2}(T-t) + \sigma_S\left(W_T^S - W_t^S\right)\right)\middle| \mathcal{F}_t\right].$$

Setting $X_t := \int_0^t x_s \mathrm{d}s$ and observing that $\int_t^T x_s \mathrm{d}s = X_T - X_t$, the previous expression rewrites as

$$\begin{aligned}F(t,T) = S_t \exp\left(\int_t^T r(s)\mathrm{d}s - \int_t^T g(s)\mathrm{d}s - \frac{\sigma_S^2}{2}(T-t)\right)\\ \times \mathbb{E}\left[\exp\left(-\left(X_T - X_t\right) + \sigma_S\left(W_T^S - W_t^S\right)\right)\middle| \mathcal{F}_t\right].\end{aligned} \tag{12}$$

In order to compute the expected value in (12), we derive in Proposition 4 the Laplace transform of the random vector $\left(W_T^S, x_T, X_T\right)$, and then we use it in Corollary 5 to compute $F(t,T)$. The proofs of both these results are deferred to Appendix B of the Appendix.

Proposition 4. *Let $\alpha, \beta, \gamma \in \mathbb{R}$. The Laplace transform of the random vector $\left(W_T^S, x_T, X_T\right)$ reads*

$$\mathbb{E}\left[\exp\left(-\alpha W_T^S - \beta x_T - \gamma X_T\right)\middle| \mathcal{F}_t\right]$$

$$\begin{aligned}&= \exp\left[-\alpha W_t^S - \left(\left(\beta - \frac{\gamma}{\kappa}\right)e^{-\kappa(T-t)} + \frac{\gamma}{\kappa}\right)x_t - \gamma X_t\right.\\ &\quad + \left(\frac{\sigma_x^2\gamma^2}{2\kappa^2} - \left(\theta - \frac{\rho\sigma_x\alpha}{\kappa}\right)\gamma\right)(T-t) + \left(\beta - \frac{\gamma}{\kappa}\right)\\ &\quad \times \left(\left(\theta - \frac{\rho\sigma_x\alpha}{\kappa}\right) - \frac{\sigma_x^2\gamma}{\kappa^2}\right)\\ &\quad \times \left(e^{-\kappa(T-t)} - 1\right)\\ &\quad - \frac{\sigma_x^2}{4\kappa}\left(\beta - \frac{\gamma}{\kappa}\right)^2\left(e^{-2\kappa(T-t)} - 1\right) + \left(\frac{\alpha^2}{2} - \lambda\right)(T-t)\\ &\quad \left. + \lambda\int_t^T h\left(B(s)\right)\mathrm{d}s\right]\end{aligned} \tag{13}$$

where

$$\begin{aligned}B(t) &= \left(b - \frac{c}{\kappa}\right)e^{\kappa t} + \frac{c}{\kappa}\\ h(\varkappa) &= \int_{supp(Y)} e^{-\varkappa y} f_Y(y)\mathrm{d}y.\end{aligned} \tag{14}$$

The joint Laplace transform derived in the previous proposition holds true for any distribution Y chosen for the i.i.d. jumps. However, notice that a closed form expression for this transform can be obtained only if the integral in (14) and, afterwords, the integral in the last term of (13) can be solved explicitly. As a matter of facts, this holds true for the centred double exponential distribution. Indeed, recalling its density function $f_Y(y)$ in (8) the integral in (14) solves as

$$\begin{aligned}h(\varkappa) &= \int_{-\infty}^{+\infty} e^{-\varkappa y}\frac{\phi}{2}\left(\exp(\phi y)\mathbf{1}_{\{y\le 0\}} + \exp(-\phi y)\mathbf{1}_{\{y>0\}}\right)\mathrm{d}y\\ &= \frac{\phi}{2}\left(\frac{1}{\phi - \varkappa} + \frac{1}{\phi + \varkappa}\right)\\ &= \frac{\phi^2}{\phi^2 - \varkappa^2}.\end{aligned}$$

Then, as far as the integral in (8) is concerned, setting $u := -(T-s)$, we get

$$\int_t^T h\left(B(s)\right)\mathrm{d}s = \int_{-(T-t)}^0 h\left(B(u+T)\right)\mathrm{d}u$$

with $B(u+T) = \left(\beta - \frac{\gamma}{\kappa}\right)e^{\kappa u} + \frac{\gamma}{\kappa}$, that delivers

$$\begin{aligned}\int_t^T h\left(B(s)\right)\mathrm{d}s &= \int_{-(T-t)}^0 h\left(B(u+T)\right)\mathrm{d}u\\ &= \int_{-(T-t)}^0 \frac{\phi}{2}\left(\frac{1}{\phi - B(u+T)} + \frac{1}{\phi + B(u+T)}\right)\mathrm{d}u\\ &= \frac{\phi}{2}\frac{1}{\gamma^2 - \kappa^2\phi^2}\left(-2\kappa^2\phi(T-t)\right.\\ &\quad + (\gamma + \kappa\phi)\ln\left[\frac{\kappa(\beta - \phi)}{\gamma + e^{-\kappa(T-t)}(-\gamma + \beta\kappa) - \kappa\phi}\right]\\ &\quad \left. + (\gamma - \kappa\phi)\ln\left[\frac{\gamma + e^{-\kappa(T-t)}(-\gamma + \beta\kappa) + \kappa\phi}{\kappa(\beta + \phi)}\right]\right).\end{aligned} \tag{15}$$

On the contrary, if $Y \sim \mathcal{N}(0, \phi^2)$, the integral in (14) can be easily computed and delivers $h(\varkappa) = \exp\left(\frac{\phi^2\varkappa^2}{2}\right)$. However, the second integral in (13) would rewrite as

$$\int_t^T \exp\left(\frac{\phi^2}{2}\left(\left(b - \frac{c}{\kappa}\right)e^{\kappa s} + \frac{c}{\kappa}\right)\right)\mathrm{d}s$$

which can be solved involving the exponential integral function that admits only numerical approximations.

Focusing on the specific case of double exponentially distributed jumps, we can now use the Laplace transform computed in Proposition 4 to retrieve the futures price in (12).

Corollary 5. *The time-t price $F(t,T)$ of a futures contract on S with maturity T reads*

$$F(t,T) = S_t \exp\left(\int_t^T r(s)\mathrm{d}s - \int_t^T g(s)\mathrm{d}s\right)\exp\left[-B(t,T)x_t + \frac{\kappa\theta + \rho\sigma_x\sigma_S}{\kappa}\right.$$

[12] For an effective recap on the main results of stochastic calculus for jump-diffusive processes see, e.g. Schönbucher (2003), Section 4.8, and the references therein.

$$\times (B(t,T)-(T-t))$$
$$+\frac{\sigma_x^2}{4\kappa^3}\left(2\kappa(T-t)-3+4e^{-\kappa(T-t)}-e^{-2\kappa(T-t)}\right)-\lambda(T-t)$$
$$+\frac{\lambda\phi}{2}\frac{1}{1-\kappa^2\phi^2}\left(-2\kappa^2\phi(T-t)+(\kappa\phi-1)\ln\left[\frac{\phi}{B(t,T)+\phi}\right]\right.$$
$$\left.-(\kappa\phi+1)\ln\left[\frac{-B(t,T)+\phi}{\phi}\right]\right)\Bigg] \tag{16}$$

where $B(t,T):=\frac{1}{\kappa}\left(1-e^{-\kappa(T-t)}\right)$.

As it will be useful in our empirical applications, we compute explicitly also the unconditional time-0 price $F(0,T)$ of a futures contract on S with maturity T.

Given the particular choice for the period function $g(\cdot)$ in (6) and letting $y(t)$ represent the yield to maturity[13] of the risk-free security, we have

$$F(0,T)=S_0\exp\left[Y(T)T-\frac{a}{b}(\sin(bT+c)-\sin(c))-\lambda T+\frac{\kappa\theta+\rho\sigma_x\sigma_S}{\kappa}\right.$$
$$\times (B(0,T)-T)-B(0,T)x_0$$
$$+\frac{\sigma_x^2}{4\kappa^3}\left(2\kappa T-3+4e^{-\kappa T}-e^{-2\kappa T}\right)+\frac{\lambda\phi}{2}\frac{1}{1-\kappa^2\phi^2}$$
$$\times\left(-2\kappa^2\phi T+(\kappa\phi-1)\ln\left[\frac{\phi}{B(0,T)+\phi}\right]\right.$$
$$\left.\left.-(\kappa\phi+1)\ln\left[\frac{-B(0,T)+\phi}{\phi}\right]\right)\right] \tag{17}$$

with $B(0,T)=\frac{1}{\kappa}\left(1-e^{-\kappa T}\right)$.

Remark 6. Although not derived in the original work of Gibson and Schwartz (1990), we can deduce the time-0 price of a futures contract on S with maturity T in the GS model with neither seasonality nor jumps, setting $a=b=c=\lambda=0$ in (17). Doing so, we obtain

$$F^{GS}(0,T)=S_0\exp\left[Y(T)T+\frac{\kappa\theta+\rho\sigma_x\sigma_S}{\kappa}(B(0,T)-T)-B(0,T)x_0\right.$$
$$\left.+\frac{\sigma_x^2}{4\kappa^3}\left(2\kappa T-3+4e^{-\kappa T}-e^{-2\kappa T}\right)\right] \tag{18}$$

3.4. Pricing of non-linear payoffs

While futures represent the most liquid instruments in natural gas financial markets, options on futures are extremely popular as well. At the TTF, standard vanilla call and put options are actively traded, with each option contract corresponding to a specific monthly futures contract. These options are characterized by a maturity that aligns precisely with the underlying futures contract's delivery date and are made available for trading up to one year prior to expiration.

As the futures price converges to the spot price at each delivery date, we can use the explicit Laplace transform derived in Proposition 4 to determine the characteristic function of $\log S_T$ and price plain vanilla options on $F(T,T)=S_T$ through the COS Method in Fang and Oosterlee (2009).

From (9), we can rewrite S_T as

$$S_T=\exp\left(\mu(T)+\sigma_S W_T^S-X_T\right) \tag{19}$$

[13] Within the framework of Svensson (1994) it holds

$$y(t)=\frac{1}{t}\left(\beta_0+\beta_1\frac{1-\exp(-t/\tau_1)}{t/\tau_1}+\beta_2\left(\frac{1-\exp(-t/\tau_1)}{t/\tau_1}-\exp(-t/\tau_1)\right)\right.$$
$$\left.+\beta_3\left(\frac{1-\exp(-t/\tau_2)}{t/\tau_2}-\exp(-t/\tau_2)\right)\right).$$

Table 3
Parameters of the market model for the Monte Carlo simulation of the trajectories in Fig. 5 and of the normalized forward curves in Fig. 6. Details of the approximated maximum-likelihood estimation of these parameters in the Appendix.

S_0	σ_S	ρ	δ_0	σ_x	κ	θ
12.75	0.9247	0.6624	0.6366	3.6136	19.5643	−0.1923
a	b	c	λ	ϕ	LogLikelihood	
0.3914	6.0338	6.1540	4.2536	0.7947	6288.03	

with $\mu(t)=\log S_0+\int_0^t(r(s)-g(s))\,ds-\frac{\sigma_S^2}{2}t$ and where $X_t=\int_0^t x_s ds$ as before. The characteristic function of $\log S_T$ can be computed as

$$\varphi_{\log S_T}(v):=\mathbb{E}\left[\exp(-iv\log S_T)\right]$$
$$=\exp(-iv\mu(T))\,\mathbb{E}\left[\exp(-iv\sigma_S W_T^S+ivX_T)\right].$$

which can be explicitly derived from the Laplace transform of (W_T^S,x_T,X_T) in Proposition 4 evaluating it at $\alpha=iv\sigma_S$, $\beta=0$, $\gamma=-iv$ with $t=0$. Once the explicit expression of the characteristic function of $\log S_T$ is obtained, we can apply the COS Method to retrieve the probability density function of $\log S_T$ and evaluate any payoff function involving S_T.[14]

Although often traded over-the-counter, Asian options on natural gas contracts are also quite popular. If the log increments of the underlying asset (either futures or spot prices) were independent, one could apply the pricing techniques proposed in Fusai and Meucci (2008), which rely on the availability of the characteristic function of the log increment of the underlying. However, the JOU process used for modelling the stochastic convenience yield disrupts the independence of these increments, making this approach inapplicable. A potential solution to this issue, which requires further analysis, is to adapt techniques developed for the pricing of Asian options under stochastic volatility models, possibly also incorporating jump components, as explored, for example, by Kyriakou et al. (2016) and Corsaro et al. (2019).

Nevertheless, the pricing of Asian options in this setting can still rely on Monte Carlo techniques. In this regard, the flexible control variate approach proposed in Dingeç et al. (2015) or the lower/upper bounds approximation in Fusai and Kyriakou (2016) can be employed to enhance computational efficiency.

3.5. Simulation of the model

We now simulate a few trajectories of the model proposed in Section 3.1 along with a few normalized forward curves in order to verify whether the model itself can reproduce the stylized features documented in Section 2.2 for the actual log spot price and convenience yield and in Section 2.1 for the actual normalized forward curves.

The simulation is performed by means of a standard Euler discretization of (3)–(5) exploiting a daily monitoring and a time horizon equal to $T=14$ years, which corresponds to the length of our sample. As far as the simulation of the trajectories are concerned, the parameters of the market model are collected in Table 3 and are derived from the two series S and $\hat{\delta}$ described in Section 2.1 using a simplified maximum likelihood-based estimation algorithm described in Appendix C of Appendix.

Fig. 5 displays two simulated trajectories of the daily log spot price $\ln S_t$ and of the convenience yield δ_t. As we can see, these trajectories are qualitatively similar to the realized ones in the top panels of Fig. 3 and display the three features outlined in Section 2.2. In particular, the

[14] Unreported numerical tests, validated against rigorous Monte Carlo-based reference estimates, demonstrate that the proposed methodology exhibits exceptional precision and near-instantaneous computational efficiency when applied to European options.

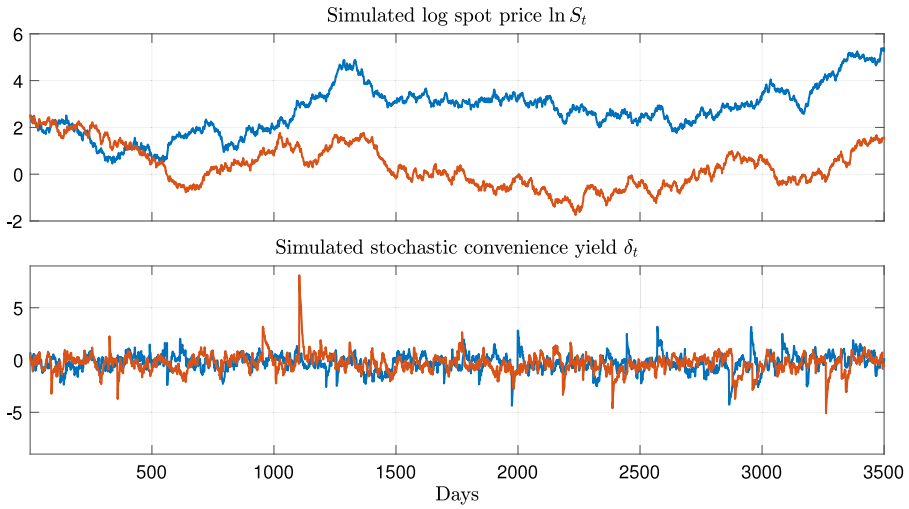

Fig. 5. Two simulated trajectories of the daily log spot price $\ln S_t$ (top panel) and of the convenience yield (bottom panel) according to the model presented in Section 3.1. Parameters of the model as in Table 3.

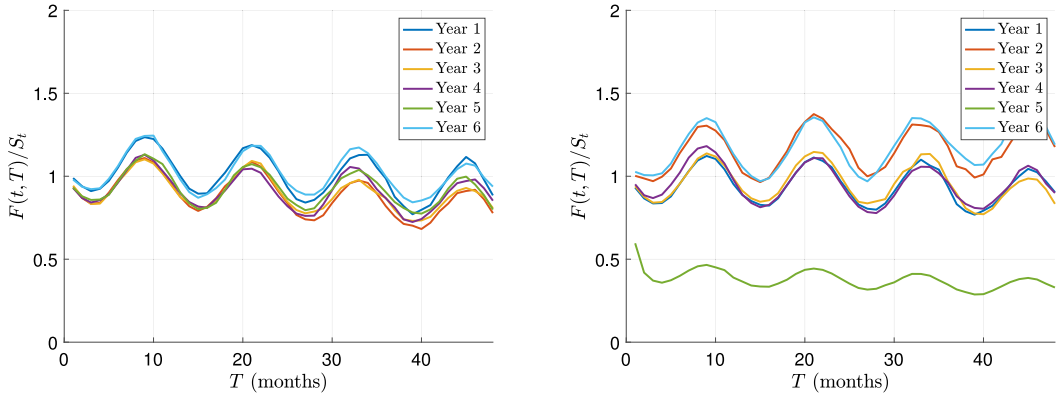

Fig. 6. Simulated normalized forward curves obtained from the Monte Carlo simulations of the model. Parameters of the model: $S_0 = 100$, $\sigma_S = 0.8$, $r(t) \equiv 0.05$, $\rho = 0.8$, $\delta_0 = 0$, $\kappa = 10$, $\theta = 0$, $\sigma_x = 2$, $a = 1$, $b = 2\pi$, $c = 0$, $\lambda = 0.4$, $\phi = 0.4$.

log spot price does not look stationary at all while the convenience yield does; the latter displays both very little persistence and several substantial spikes that are absorbed quite quickly; finally, the convenience yield features a mild seasonal behaviour, which is slightly hidden by the large volatility of its mean-reverting component.

We now verify whether the proposed model can also reproduce the features of the normalized forward curves described in Section 2.1, using a set of parameters inspired from the output of the futures curve calibrations in the next section.

In the left panel of Fig. 6 we randomly select a reference day within the first year of daily simulations. Then, we plot the normalized forward curves[15] for that day and for the same day of the following five years. In this way, we can replicate the structure of Fig. 2 that was displaying the normalized forward curves at the first trading day (so, the reference day there was January, 2) of each year. As we can see, the behaviour of the curves in the left panel of Fig. 6 is rather stable as they fluctuate periodically around one. Overall, we can conclude that the graph matches the left panel of Fig. 2.

For the right panel of Fig. 6, the reference day is not chosen randomly. Instead, it is specifically selected so that either on that day or within the following five anniversaries, the largest simulated jump in the convenience yield occurs. In this way we can visualize what happens to a normalized forward curve when the convenience yield jumps. As we can see, when a jump hits the convenience yield (like on the reference day of Year 5 in the right panel of Fig. 6) the normalized forward curve deviates significantly from one and then fluctuates periodically around a different value. This is consistent with the observed behaviour of the normalized forward curves in the right panel of Fig. 2 and it can be obtained only by brining in a discontinuous convenience yield.

3.6. Jumps in the spot price

As shown in Figs. 3 and 4, the spot price process S also appears to exhibit a jump component, albeit of a smaller magnitude compared to the jumps observed in the implied convenience yield $\hat{\delta}$. To account for this, we modify the $\mathbb{Q}$-dynamics of S as defined in (3) to

$$\frac{\mathrm{d}S_t}{S_{t^-}} = \left(r(t) - \delta_t - \lambda^S m_J\right)\mathrm{d}t + \sigma_S \mathrm{d}W_t^S + \mathrm{d}J_t^S \tag{20}$$

where $J^S = \left(J_t^S\right)_{t\geq 0}$, with $J_t^S = \sum_{j=1}^{N_t^S}(Y_j^S - 1)$, is a compound Poisson process with intensity $\lambda^S \in \mathbb{R}^+$ and where the Y_j^S's are i.i.d. random variables representing the jumps affecting the spot price process. Here $m_J = \mathbb{E}\left[Y_j^S\right] - 1$.

First, it is important to highlight that, regardless of the specific distribution of the jumps Y^S's, the pricing formula in (17) and the

[15] These forward curves are computed out of six independent sets of Monte Carlo simulations with initial values for S and δ equal to the values of the processes along the original trajectories at the chosen day and at the following five anniversaries.

Table 4
Maximum likelihood-based estimate of the parameters of the market model defined by (20)-(4)-(5). The details of the estimation routine are provided in the Appendix.

	S_0	σ_S	ρ	δ_0	σ_x	κ	θ
A	12.75	0.9256	0.6665	0.6366	3.6641	11.2747	−0.2041
B		0.8221	0.6724		3.8192	1.3067	−1.5279

	a	b	c	λ	ϕ	λ^S	σ_J	LogLikelihood
A	−0.4809	5.9986	−9.2751	4.3222	0.7301	0.0000	3.2397	6272.68
B	0.1986	5.8849	2.6171	–	–	2.783	0.2534	4210.80

model's calibration results remain unchanged for futures contracts. Since futures payoffs are linear in S, the compensator term $\lambda^S m_J$ of the compound Poisson process J^S offsets any contribution of the jump component to the expected value of S.

To analyse the magnitude of the spot price jump component in the time series, we employ the approximated maximum likelihood estimation method introduced in Section 2.2 and further detailed in Appendix C. For this analysis, we follow the widely adopted jump–diffusion model of Merton (1976), assuming that the jumps Y_j^S follow a lognormal distribution. Specifically, we assume that the logarithm of the jumps is normally distributed with zero expected value and variance σ_J^2, that implies $m_J = e^{\frac{\sigma_J^2}{2}} - 1$. This assumption limits the increase in model complexity to just two additional parameters: λ^S and σ_J.

Table 4 presents the results of the maximum likelihood estimation of the model's parameters. Row A refers to the model in which both S and δ are allowed to jump. Notably, despite the fact that the standard deviation σ_J of the jump component in S is more than twice the volatility σ_S of the Brownian shock, the estimated jump intensity λ^S is close to zero.[16] This suggests that the small spikes observed in the spot price process can be attributed to abnormally large realizations of W^S. Consistently, the overall log-likelihood of the model remains virtually identical to that reported in Table 3, which was obtained without incorporating the additional jump component.

Row B of Table 4 corresponds to the model specification in which only the spot price process, S, is allowed to exhibit jumps. As observed, this specification results in a higher estimated jump intensity, λ^S, accompanied by a relatively small jump standard deviation, σ_J. However, the log-likelihood of the model decreases significantly, indicating that the observed spikes in the convenience yield cannot be adequately captured by Brownian shocks alone.

Having qualitatively demonstrated that the proposed model can replicate the key characteristics of the European natural gas market, we now test the model's fit to futures prices using the explicit formula derived in Corollary 5. Additionally, we investigate the optimal calibrated parameters and evaluate the significance of both the seasonal and jump components of the convenience yield.

4. Empirical analysis

In this section we bring our model to the data. In particular, in Section 4.1 we fit the model to the observed forward curves, during both a pre- and a post-COVID-19/Russia–Ukraine period. Then, in Section 4.2, we analyse the results studying the determinants of the forward curves.

4.1. Fit of the actual forward curve

We now evaluate how well the proposed model fits the forward curves by comparing the futures prices generated by our model (using Eq. (17) for different maturities) to actual forward prices for a sample of days from both a pre- and a post-2020 period. For sake of a full comparison, we also fit the forward curves generated by the GS model, using the futures price formula in (18), assuming no seasonality or jumps.

The parameters we need to determine for the full model are $\Theta = (\sigma_S, \rho, \delta_0, \sigma_x, \kappa, \theta, a, b, c, \lambda, \phi)$, while the parameters included in the GS model are $\Theta^{GS} = (\sigma_S, \rho, \delta_0, \sigma_x, \kappa, \theta)$. Once a specific trading day is selected, we set that day as $t = 0$ and retrieve the current spot price, which becomes our S_0, and the current forward curve $\{F^{mkt}(0, T_i)\}_i$. Despite futures prices being quoted for monthly maturities up to ten years, we fit the models using futures prices with maturities less than two years, which are the most liquid. However, we also include a single four-year contract to capture the long-run trend of the curve. Therefore, we have $\{T_i\}_i = \{\frac{j}{12}\}_{j=1,\dots,24} \cup \{4\}$ which implies that we fit the models to twenty-five futures prices. As usual, we use the mean squared error as the objective function and, on a daily basis, we fit the models to the actual curves solving[17]

$$\hat{\Theta} := \underset{\Theta \in D}{\arg\min} \quad \frac{1}{25} \sum_i \left(F^{mkt}(0, T_i) - F(0, T_i; \Theta) \right)^2 \tag{21}$$

for the full model and replacing Θ by Θ^{GS} and $F(0, T_i; \Theta)$ by $F^{GS}(0, T_i; \Theta^{GS})$ for the GS model and where D represents the domain[18] of the parameters.

4.2. Analysis of the results

Tables 5 and 6 display the results of this fit exercises for the first trading day of each quarter of 2012 and 2022 respectively.

4.2.1. Goodness of fit

First of all, we notice that the residual mean squared error (res. MSE) in the second-last row of the two tables, namely the value of the objective function at the optimum, is always larger for the original GS model. Despite this being a mechanical consequence of the fact that the full model involves five more parameters than the GS one, Table 7 shows that the full model displays a residual error which is always at least one order of magnitude smaller than the one from the GS model. The last row of Tables 5 and 6 reports the "out-of-sample" mean squared error (OOS MSE) which corresponds to the mean squared error on the second part of the forward curves (namely the forward contracts with maturities from twenty-five to forty-seven months) between the actual futures prices and the ones obtained with the two models. Although these contracts are less liquid due to their relatively long maturities, we see that the full model delivers a better fit (but for October 1, 2012 and July 1, 2022) also for future prices not included as in input.

The size of the residual mean squared errors is inversely proportional to the goodness of fit of the forward curves. Figs. 7 and 8 show the actual and the fitted forward curves for the same days already considered in Tables 5 and 6. In particular, the graphs display both the first part of the curve (up to $T = 24$ months) used as an input for the calibration and the "out-of-sample" part. As we can see, the full model can capture the plain seasonal behaviour of the (normalized) forward curves that arise clearly in Fig. 7 for 2012 as well as the unusual shapes of the curves displayed in Fig. 8 for 2022. On the contrary, the GS model without any seasonality and jump component, can only capture the trend of the curves.

[16] The estimated value for λ^S is 2×10^{-8}. Interestingly, in other local minima of the maximum likelihood objective function, which yield similar optimal values, λ^S exceeds 3. However, in these cases, the corresponding standard deviation of the jumps, σ_J, is below 0.1, while σ_S remains nearly unchanged. Consequently, even in these scenarios, the contribution of the jump component is negligible compared to that of the Brownian shock W^S.

[17] In order to highlight how the objective function depends on the controls, we add the explicit dependence of the futures prices in (17) and in (18) on the parameters in Θ/Θ^{GS}.

[18] In our numerical experiments we set $D = ([0.05, 4], [-1, 1], [-4, 4], [0.05, 4], [0.05, 40], [-4, 4], [-12, 12], [-12, 12], [-12, 12], [0, 3], [0.1, 5])$ and we repeat the optimization routine 25 times starting from different initial guesses drawn from a multivariate uniform distribution over D.

Table 5
Optimal parameters and residual errors from the fit of the actual forward curves in (21) at the first trading day of each quarter of 2012.

S_0	January 2, 2012		April 2, 2012		July 2, 2012		October 1, 2012	
Model	21.00		25.30		24.02		25.75	
	Full	GS	Full	GS	Full	GS	Full	GS
σ_S	1.6941	2.1600	1.2406	1.9493	0.7538	0.5774	2.7418	2.5327
ρ	0.2180	0.0673	−0.6533	−0.1156	0.7267	0.7248	0.5190	0.0843
δ_0	−0.8407	−0.3257	−0.9355	−0.2477	−0.0165	−0.3228	−0.1061	−0.1505
σ_x	2.0433	0.5868	2.1747	0.6098	0.0631	1.3538	0.0531	0.5238
κ	1.8560	0.6134	5.5423	1.0045	0.4317	1.9189	0.0525	1.7142
θ	0.2414	0.2798	0.8583	0.3678	−0.0343	−0.0055	−0.0428	−0.0019
a	−0.4874	–	−0.5642	–	0.4112	–	0.3493	–
b	−6.4043	–	−6.4394	–	−6.5265	–	6.1786	–
c	−7.7931	–	−9.3094	–	4.9926	–	−2.9692	–
λ	1.4378	–	1.8176	–	0.012	–	0.0094	–
ϕ	3.2270	–	0.4051	–	4.5152	–	3.6125	–
$V[Y]$	0.1921	–	12.1897	–	0.0981	–	0.1533	–
res. MSE	0.1224	1.6581	0.1388	2.4934	0.1023	1.4072	0.0576	1.1301
OOS MSE	0.7633	5.9563	0.3128	2.7081	0.3635	3.0458	2.8741	2.0204

Table 6
Optimal parameters and residual errors from the fit of the actual forward curves in (21) at the first trading day of each quarter of 2022.

S_0	January 3, 2022		April 1, 2022		July 1, 2022		October 3, 2022	
Model	78.5		121.9		149.75		163.5	
	Full	GS	Full	GS	Full	GS	Full	GS
σ_S	2.7720	2.2446	2.5110	2.5966	3.1328	1.6192	1.7455	0.7979
ρ	0.3126	0.3649	0.5363	0.5379	0.2666	0.5124	0.8317	0.9341
δ_0	−0.3378	0.2099	−2.1287	−0.7817	−0.1141	−0.5521	−1.5100	−0.8896
σ_x	0.0528	0.5915	0.3609	2.6573	0.9688	3.2884	0.4518	1.5732
κ	1.0970	0.0500	3.2539	0.8489	5.9391	1.4179	1.4992	0.5316
θ	1.4627	0.1232	1.5279	0.3789	0.5810	1.0494	1.1593	1.9964
a	0.9853	–	1.0205	–	−0.8449	–	−0.7210	–
b	−5.5800	–	6.7375	–	−6.9373	–	−5.6030	–
c	0.5610	–	−0.5742	–	2.1438	–	−1.1055	–
λ	0.5507	–	0.0876	–	0.0035	–	0.3956	–
ϕ	1.0401	–	0.3161	–	0.1693	–	0.7556	–
$V[Y]$	1.8489	–	20.0131	–	69.7934	–	3.5026	–
res. MSE	13.3929	56.2995	29.9510	97.9441	8.8720	77.5843	41.8979	193.8212
OOS MSE	6.1735	7.9256	15.9796	27.6193	19.4165	9.9247	90.2762	177.0520

Table 7
Average residual mean squared error from daily fits of the forward curves according the GS model and the full proposed model.

	GS model	full model
2010	0.7422	0.1017
2011	1.0885	0.1067
2012	1.4728	0.0922
2013	0.8871	0.1234
2014	0.8475	0.0997
2015	0.5046	0.0398
2016	0.3562	0.0226
2017	0.5630	0.0314
	GS model	full model
2018	1.7791	0.1398
2019	1.7094	0.1951
2020	1.0690	0.0774
2021	27.6739	6.4865
2022	114.5231	34.1966
2023	8.3268	1.2153
2024	2.4503	0.2175

4.2.2. Seasonal component

As we can see from Figs. 7 and 8, the periodic component of the model seems necessary to reproduce the seasonality in the (normalized) forward curves. As far as the parameters of the periodic function $g(t)$ introduced in (6) are concerned, we notice that the frequency of the seasonal component, defined as $|b|/(2\pi)$, is almost 1 unit of time, i.e. one year, since the absolute value of b is always quite close to 2π. This is particularly true for 2012, when the seasonal pattern of the forward curves is in plain sight while is a little less so for 2022, when forward curves are much more irregular. However, this behaviour is not surprising since demand and supply for natural gas have stable annual patterns. The actual sign of b might change as the signs of a and b are hardly identifiable. Indeed, we see that the absolute values of a and b are quite stable across all dates of the same year and across the two different models, whereas their signs are not. In particular, their product is always negative, but their individual signs keep changing.

4.2.3. Jump component

Finally, we document that the contribution of the jump component is significantly more pronounced in 2022, when forward curves exhibit substantial deviations from their usual regular patterns, compared to 2012, when they remain relatively stable. This effect can be quantified by the variance of each jump Y, which, recalling the density of the double exponential distribution in (8), is given by $\frac{2}{\phi^2}$. As shown in Tables 5 and 6, the average variance of the jump distribution across the four selected dates in 2012 is 3.16, with an average jump intensity of 0.82. In contrast, for 2022, the average variance of the jump component increases significantly to 23.79, while the average jump intensity is reduced to 0.26. Despite the lower estimated jump frequency, the exceptionally high variance of jumps plays a crucial role in capturing

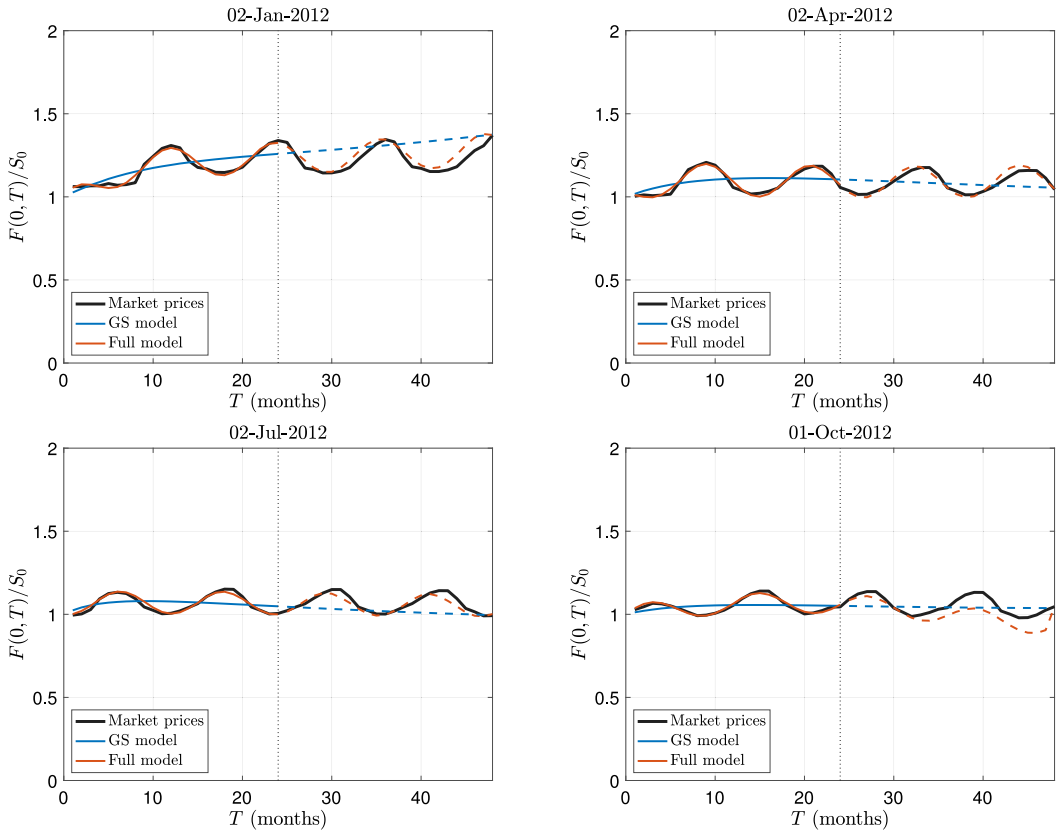

Fig. 7. Fit of the forward curves of the pure (Gibson and Schwartz, 1990) model (GS model) and the proposed model (Full model) for the first trading day of January, April, July and October, 2012. The contracts with maturities less than two years (namely the ones on the left of the vertical dashed black line) and the one with forty-eight maturity are used as an input in the calibration routine.

the atypical fluctuations in the forward curves and their departures from standard seasonal effects.

5. Conclusion

In the present paper we investigated the European natural gas spot and futures markets. In particular, we started from an empirical analysis of the time series of the natural gas log spot price and of its implied convenience yield. This analysis showed that the series of log spot price is not stationary while the one of the convenience yield is and that both a seasonal factor and a jump component are more evident in the series of the convenience yield rather than in the one of log spot prices. Following this evidence and in the spirit of Gibson and Schwartz (1990) we propose a two-factor no-arbitrage model where the convenience yield is built as the sum of a deterministic seasonal factor and a jump component. When fitted to data, our model performed well and was able to reproduce the standard behaviour of natural gas forward curves in the pre COVID-19/Russia–Ukraine war period as well as the unusual shapes of the curves after that have been in place after those disruptive events.

This research offers several potential avenues for further investigation, particularly in the context of pricing applications. First, an important direction would be to examine the pricing of path-dependent options, such as Asian options. Furthermore, it would be valuable to assess whether the model, when calibrated to a specific forward curve, can accurately predict the prices of options written on futures contracts associated with that curve. In this context, the jump component of the convenience yield, which indirectly affects skewness and kurtosis, is expected to play a crucial role. Moreover, incorporating time-varying jump intensity and/or seasonality parameters would constitute a significant enhancement to the model.

CRediT authorship contribution statement

Francesco Rotondi: Writing – review & editing, Writing – original draft, Visualization, Validation, Supervision, Software, Resources, Project administration, Methodology, Investigation, Funding acquisition, Formal analysis, Data curation, Conceptualization.

Acknowledgements

I would like to thank the two anonymous Reviewers for their insightful comments on earlier versions of this paper. I am also grateful to Anna Battauz for valuable discussions on the topics addressed, as well as to the participants of the Energy Finance Italy 9 conference held at the University of Bari (February 2024) and the 48th AMASES Annual Conference hosted by the University of Naples in Ischia (September 2024). All remaining errors are my sole responsibility.

Appendix

This Appendix comprises the following sections: the analysis of the model under the physical measure $\mathbb{P}$, explicitly incorporating risk premia (Appendix A); the proofs of the propositions presented in the main text (Appendix B); the description of the approximate maximum likelihood-based estimation of the baseline model, extended to account for jumps in the spot price as discussed in Section 3.6 (Appendix C).

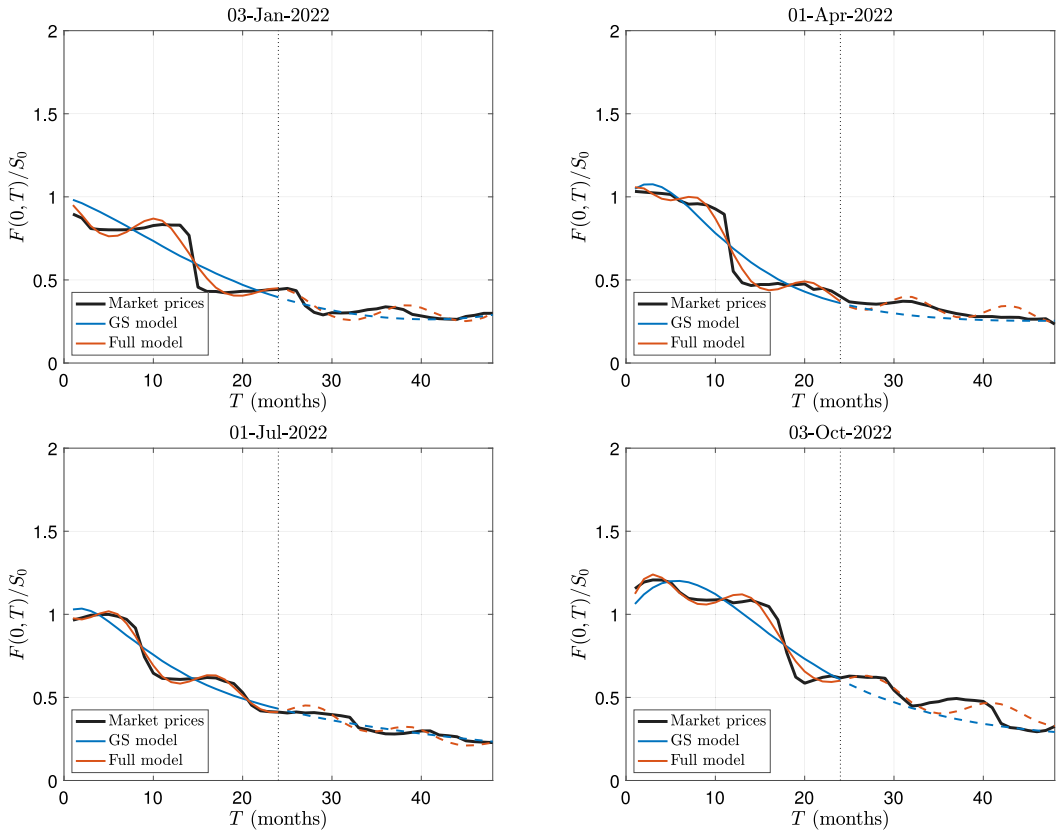

Fig. 8. Fit of the forward curves of the pure (Gibson and Schwartz, 1990) model (GS model) and the proposed model (Full model) for the first trading day of January, April, July and October, 2022. The contracts with maturities less than two years (namely the ones on the left of the vertical dashed black line) and the one with forty-eight maturity are used as an input in the calibration routine.

Appendix A. $\mathbb{P}$-dynamics of the model

As the primary focus of this paper is futures pricing, the proposed model has been introduced under a specific risk-neutral probability measure $\mathbb{Q}$. However, an analysis of the same dynamics under the physical measure $\mathbb{P}$ may yield valuable insights into the market prices of risks and the determinants of the shape of futures curves. However, as noted by Schwartz and Smith (2000) and Geman and Nguyen (2005) among others, additional subjective assumptions are required to estimate these risk premia from observed data.

In the following, quantities denoted by $\tilde{\cdot}$ refer to the physical measure $\mathbb{P}$, while the risk-free interest rate r is assumed constant for simplicity.

Let $\tilde{W}^S = (\tilde{W}_t^S)_{t\geq 0}$ and $\tilde{W}^x = (\tilde{W}_t^x)_{t\geq 0}$ denote two standard Brownian motions under $\mathbb{P}$, satisfying $\mathrm{d}\langle \tilde{W}^S, \tilde{W}^x\rangle_t = \rho \mathrm{d}t$ and representing the two (correlated) diffusive risk factors of the model: the spot price risk factor and the convenience yield one. To isolate the individual contributions of these risks, let $\tilde{W}^{x*} = (\tilde{W}_t^{x*})_{t\geq 0}$ be a standard Brownian motion under $\mathbb{P}$, uncorrelated with $\tilde{W}^S$, such that $\mathrm{d}\tilde{W}_t^x = \rho \mathrm{d}\tilde{W}_t^S + \sqrt{1-\rho^2}\mathrm{d}\tilde{W}_t^{x*}$. In this way, $\tilde{W}^{x*}$ represents the component of convenience yield risk that is uncorrelated with the spot price one. Additionally, let $\tilde{J} = (\tilde{J}_t)_{t\geq 0}$ be a compound Poisson process under $\mathbb{P}$, independent of both $\tilde{W}^S$ and $\tilde{W}^{x*}$, with intensity $\tilde{\lambda} \in \mathbb{R}^+$, where the i.i.d. jumps Y_j have probability density function $f_Y(y)$.

Under $\mathbb{P}$, we assume that the model dynamics are given by

$$\begin{aligned} \frac{\mathrm{d}S_t}{S_t} &= \tilde{\mu}\mathrm{d}t + \sigma_S \mathrm{d}\tilde{W}_t^S, \\ \mathrm{d}\delta_t &= g'(t)\mathrm{d}t + \mathrm{d}x_t, \\ \mathrm{d}x_t &= \kappa\left(\tilde{\theta} - x_{t^-}\right)\mathrm{d}t + \sigma_x \mathrm{d}\tilde{W}_t^x + \mathrm{d}\tilde{J}_t, \end{aligned} \tag{22}$$

where $\tilde{\mu}$ represents the physical expected growth rate of the spot price, $\tilde{\theta}$ the physical long-run mean of x and where the other parameters (that will coincide under $\mathbb{P}$ and $\mathbb{Q}$ due to the precise change of measure we will consider) are defined in Section 3.1.

To transition to the risk-neutral measure $\mathbb{Q}$, we apply Girsanov's theorem, which ensures that there exists a probability measure $\mathbb{Q} \sim \mathbb{P}$ under which $W^S = (W_t^S)_{t\geq 0}$, $W^{x*} = (W_t^{x*})_{t\geq 0}$, defined through

$$\begin{aligned} \mathrm{d}W_t^S &= \vartheta_t^S \mathrm{d}t + \mathrm{d}\tilde{W}_t^S \\ \mathrm{d}W_t^{x*} &= \vartheta_t^{x*}\mathrm{d}t + \mathrm{d}\tilde{W}_t^{x*}, \end{aligned} \tag{23}$$

are two uncorrelated $\mathbb{Q}$-standard Brownian motions, for any choice of the adapted processes $\vartheta^S = (\vartheta_t^S)_{t\geq 0}$ and $\vartheta^{x*} = (\vartheta_t^{x*})_{t\geq 0}$, satisfying standard integrability conditions. Moreover, the theorem ensures that, for any choice of $\vartheta^J \in \mathbb{R}^+$, $J = (J_t)_{t\geq 0}$ is a compound Poisson process under probability $\mathbb{Q}$, independent of W^S and W^{x*}, with intensity $\lambda = \vartheta^J \tilde{\lambda}$ and i.i.d. jumps Y_j's characterized by the density function $f_Y(y)$.

The processes ϑ^S and ϑ^{x*}, together with the constant $\vartheta^J \in \mathbb{R}^+$, represent the market prices of risk associated respectively with the spot price, the component of the convenience yield risk that is uncorrelated with the spot price one, and the jumps in the convenience yield.

In order to ensure that $\mathbb{Q}$ is a risk-neutral probability, we impose the no-arbitrage condition on the spot price of the natural gas, which is a traded asset. Using Eq. (22), the stochastic differential of the discounted gain process $G = (G_t)_{t\geq 0}$ from holding one unit of S is

$$\begin{aligned} \mathrm{d}G_t &= \mathrm{d}\left(e^{-rt}S_t\right) + e^{-rt}S_t\delta_t\mathrm{d}t \\ &= e^{-rt}S_t\left((\tilde{\mu} - r)\,\mathrm{d}t + \sigma_S \mathrm{d}\tilde{W}_t^S + \delta_t \mathrm{d}t\right). \end{aligned}$$

Switching to the risk-neutral measure $\mathbb{Q}$ using (23) and rearranging terms, we obtain

$$\mathrm{d}G_t = e^{-rt}S_t\left(\left(\tilde{\mu} - r + \delta_t - \sigma_S\vartheta_t^S\right)\mathrm{d}t + \sigma_S \mathrm{d}W_t^S\right).$$

The standard no-arbitrage condition requires G to be a $\mathbb{Q}$-martingale, which commands

$$\vartheta_t^S = \frac{\tilde{\mu} - r + \delta_t}{\sigma_S}. \tag{24}$$

Now that we have explicitly formulated the model under both $\mathbb{P}$ and $\mathbb{Q}$, detailed the change of measure between them and derived the no-arbitrage restriction, we can establish the relationship between the parameters of the $\mathbb{P}$-dynamics and those of the $\mathbb{Q}$-dynamics.

As for the spot price process, substituting (23) and (24) into the first equation in (22), gives

$$\begin{aligned}\frac{\mathrm{d}S_t}{S_t} &= \tilde{\mu}\mathrm{d}t + \sigma_S\left(\mathrm{d}W_t^S - \frac{\tilde{\mu} - r + \delta_t}{\sigma_S}\mathrm{d}t\right)\\ &= \left(r - \delta_t\right)\mathrm{d}t + \sigma_S \mathrm{d}W_t^S,\end{aligned}$$

that coincides with (3).

As for x, we first notice that thanks to the identity

$$\begin{aligned}\rho\mathrm{d}\tilde{W}_t^S + \sqrt{1-\rho^2}\mathrm{d}\tilde{W}_t^{x*} &= \rho\left(\mathrm{d}W_t^S - \vartheta_t^S\mathrm{d}t\right) + \sqrt{1-\rho^2}\left(\mathrm{d}W_t^{x*} - \vartheta_t^{x*}\mathrm{d}t\right)\\ &= -\left(\rho\vartheta_t^S + \sqrt{1-\rho^2}\vartheta_t^{x*}\right)\mathrm{d}t + \rho\mathrm{d}W_t^S\\ &\quad + \sqrt{1-\rho^2}\mathrm{d}W_t^{x*}\end{aligned}$$

we can define the $\mathbb{Q}$-Brownian motion $W^x = (W_t^x)_{t\geq 0}$ as $\mathrm{d}W_t^x = \rho\mathrm{d}W_t^S + \sqrt{1-\rho^2}\mathrm{d}W_t^{x*}$, which satisfies $\mathrm{d}\langle W^S, W^x\rangle_t = \rho\mathrm{d}t$, leading to

$$\mathrm{d}W_t^x = \left(\rho\vartheta_t^S + \sqrt{1-\rho^2}\vartheta_t^{x*}\right)\mathrm{d}t + \mathrm{d}\tilde{W}^x. \tag{25}$$

Using the third equation in (22), the fact that investors require no compensation for the convenience jump risk (that implies $\theta^J = 1$) and (25), we obtain

$$\begin{aligned}\mathrm{d}x_t &= \kappa\left(\tilde{\theta} - x_{t^-}\right)\mathrm{d}t + \sigma_x\left(\mathrm{d}W_t^x - \left(\rho\vartheta_t^S + \sqrt{1-\rho^2}\vartheta_t^{x*}\right)\mathrm{d}t\right) + \mathrm{d}J_t\\ &= \kappa\left(\tilde{\theta} - \frac{\sigma_x}{\kappa}\left(\rho\vartheta_t^S + \sqrt{1-\rho^2}\vartheta_t^{x*}\right) - x_{t^-}\right)\mathrm{d}t + \sigma_x\mathrm{d}W_t^x + \mathrm{d}J_t\end{aligned}$$

which matches (5) for

$$\theta = \tilde{\theta} - \frac{\sigma_x}{\kappa}\left(\rho\vartheta_t^S + \sqrt{1-\rho^2}\vartheta_t^{x*}\right). \tag{26}$$

This equation represents the link between the historical long-run mean of the non-seasonal component of the convenience yield x and its risk-neutral counterpart.

Since the model is now fully characterized under $\mathbb{P}$ as well, we can finally comment on the relationship between the two uncorrelated market prices of risk, ϑ_t^S and ϑ_t^{x*}, and the phenomenon of market normal backwardation (resp. contango), that is, the situation in which the expected spot price under the physical measure, $\mathbb{E}^{\mathbb{P}}\left[S_T\right]$, exceeds (resp. is lower than) the futures price $F(0,T)$.

According to (22), the $\mathbb{P}$-expected spot price is simply given by $\mathbb{E}^{\mathbb{P}}\left[S_T\right] = S_0 e^{\tilde{\mu}T}$, where $\tilde{\mu}$ is linked to ϑ_t^S only, through (24). As for the futures price, Eq. (17), derived under $\mathbb{Q}$, shows that within our model $F(0,T)$ is directly proportional to the factor $\theta\left(B(0,T) - T\right)$. Using (26), we find that, in $\mathbb{P}$-terms, $F(0,T)$ is directly proportional to

$$\left(\tilde{\theta} - \frac{\sigma_x}{\kappa}\left(\rho\vartheta_t^S + \sqrt{1-\rho^2}\vartheta_t^{x*}\right)\right)\left(B(0,T) - T\right),$$

which shows that $F(0,T)$ is linked both to ϑ_t^S and ϑ_t^{x*}.

We first focus on ϑ_t^{x*}, as the market price of convenience yield risk uncorrelated to the spot price one impacts only $F(0,T)$. Since $B(0,T) - T < 0$ for any T and as $\sigma_x > 0$, $\kappa > 0$, $\sqrt{1-\rho^2} \geq 0$, it follows that, all else being equal, a lower ϑ_t^{x*} tends to lower futures prices, thus favouring normal backwardation. Indeed, a lower market price of convenience yield risk implies that investors require little compensation for bearing this risk. As a result, the expected long-run convenience yield under the risk-neutral measure increases, thereby depressing futures prices, since holding the physical commodity becomes relatively more attractive than holding the futures contract.

In contrast, the effect of the market price of spot price risk ϑ_t^S on the futures curve is more nuanced as ϑ_t^S impacts both $F(0,T)$ and $\mathbb{E}^{\mathbb{P}}\left[S_T\right]$.

If $\rho > 0$, which is the typical situation and is also confirmed by the empirical analysis, a lower ϑ_t^S reduces the futures price as before, thus promoting normal backwardation. On the other hand, a lower ϑ_t^S simultaneously reduces the expected spot price, since $\tilde{\mu} = \sigma_S\vartheta_t^S + r - \delta_t$, which tends to favour contango. Therefore, when $\rho > 0$, the overall impact of ϑ_t^S on the shape of the futures curve depends on the interplay between these opposing effects.

Conversely, in the less common case where $\rho < 0$, the dynamics change: a lower ϑ_t^S tends to increase the futures price while still depressing the expected spot price, both effects now contributing to favouring contango. This highlights how the correlation between spot price and convenience yield risk plays a critical role in determining the structure of the futures curve.

Appendix B. Proof of the propositions

Proof of Proposition 4. In order to derive the Laplace transform of the random vector $\left(W_T^S, x_T, X_T\right)$, we first look for the deterministic real-valued functions $A(t), B(t), C(t), D(t)$ that make the process

$$\exp\left(-A(t)W_t - B(t)x_t - C(t)X_t - D(t)\right)$$

a $\mathbb{Q}$-martingale with respect to $\mathbb{F}$.

First of all, we need to compute the infinitesimal generator of a generic deterministic function $f(t,W,x,X) : \mathbb{R}^+\times\mathbb{R}\times\mathbb{R}\times\mathbb{R} \mapsto \mathbb{R}$ applied to $\left(t, W_t^S, x_t, X_t\right)$. According to the Itô's formula for jump-diffusive processes we have

$$\begin{aligned}\mathrm{d}f(t,W_t^S,x_t,X_t) &= f_t\mathrm{d}t + f_W\mathrm{d}W_t^S + f_x\mathrm{d}x_t^c + f_X\mathrm{d}X_t\\ &\quad + \left(\int_{-\infty}^{+\infty} f(t,W_t^S,x_{t^-}+y,X_t)\mathrm{d}F_Y(y)\right.\\ &\quad \left. - f(t,W_t^S,x_{t^-},X_t)\right)\Delta N_t\\ &\quad + \frac{1}{2}f_{WW}\mathrm{d}\left\langle W^S, W^S\right\rangle_t + \frac{1}{2}f_{xx}\mathrm{d}\left\langle x^c, x^c\right\rangle_t\\ &\quad + \frac{1}{2}f_{XX}\mathrm{d}\left\langle X, X\right\rangle_t\\ &\quad + f_{WX}\mathrm{d}\left\langle W^S, X\right\rangle_t + f_{Wx}\mathrm{d}\left\langle W^S, x^c\right\rangle_t\\ &\quad + f_{xX}\mathrm{d}\left\langle x^c, X\right\rangle_t\\ &= \left(f_t + f_x\kappa\left(\theta^{\mathbb{Q}} - x_{t^-}\right) + f_X x_{t^-} + \frac{1}{2}f_{WW} + \frac{1}{2}f_{xx}\sigma_x^2\right.\\ &\quad + f_{Wx}\rho\sigma_x\\ &\quad + \lambda\left(\int_{-\infty}^{+\infty} f(t,W_t^S,x_{t^-}+y,X_t)\mathrm{d}F_Y(y)\right.\\ &\quad \left.\left. - f(t,W_t^S,x_{t^-},X_t)\right)\mathrm{d}t\right)\\ &\quad + \left(\int_{-\infty}^{+\infty} f(t,W_t^S,x_{t^-}+y,X_t)\mathrm{d}F_Y(y)\right.\\ &\quad \left. - f(t,W_t^S,x_{t^-},X_t)\right)\\ &\quad \times\left(\Delta N_t - \lambda\mathrm{d}t\right)\\ &\quad + f_W\mathrm{d}W_t^S + f_x\sigma_x\mathrm{d}W_t^x.\end{aligned}$$

Therefore, the infinitesimal generator of interest reads

$$\begin{aligned}\mathcal{A}f(t,W_t^S,x_{t^-},X_t) &= f_t + f_x\kappa\left(\theta - x_t\right) + f_X x_{t^-} + \frac{1}{2}f_{WW} + \frac{1}{2}f_{xx}\sigma_x^2 + f_{Wx}\rho\sigma_x\\ &\quad + \lambda\left(\int_{-\infty}^{+\infty} f(t,W_t^S,x_{t^-}+y,X_t)\mathrm{d}F_Y(y) - f(t,W_t^S,x_{t^-},X_t)\right).\end{aligned}$$

In order for $f(t,W,x,X) = \exp\left(-A(t)W - B(t)x - C(t)X + D(t)\right)$ to be a martingale, it must be $\mathcal{A}f(t,W,x,X) = 0$. Since

$$\begin{aligned}\mathcal{A}f(t,W,x,X) &= f(t,W,x,X)\left(-A'(t)W - B'(t)x - C'(t)X + D(t)'\right.\\ &\quad \left. - B(t)\kappa\left(\theta - x\right) - C(t)x\right.\end{aligned}$$

$$+\frac{1}{2}A(t)^2+\frac{1}{2}\sigma_x^2B(t)^2+\rho\sigma_xA(t)B(t)+\lambda\left(h\left(B(t)\right)-1\right)\Big),$$

with

$$h(\varkappa)=\int_{-\infty}^{+\infty}e^{-\varkappa y}\mathrm{d}F_Y(y).$$

we need to solve

$$\begin{aligned}&-A'(t)W-B(t)'x-C'(t)X+D'(t)-B(t)\kappa(\theta-x)-C(t)x++\frac{1}{2}A(t)^2\\&+\frac{1}{2}\sigma_x^2B(t)^2\\&+\rho\sigma_xA(t)B(t)+\lambda\left(h\left(B(t)\right)-1\right)=0\end{aligned}$$

with respect to $A(t)$, $B(t)$, $C(t)$ and $D(t)$.

Trying $A(t)=a\in\mathbb{R}$ and $C(t)=c\in\mathbb{R}$, we have

$$\begin{aligned}&-B'(t)x+D'(t)-B(t)\left(\kappa(\theta-x)-\rho\sigma_xa\right)-cx+\frac{1}{2}\sigma_x^2B(t)^2\\&+\lambda\left(h\left(B(t)\right)-1+\frac{1}{2}\frac{a^2}{\lambda}\right)=0\end{aligned}$$

that is solved by

$$\begin{aligned}B(t)&=\left(b-\frac{c}{\kappa}\right)e^{\kappa t}+\frac{c}{\kappa}\\D(t)&=\left(\left(\theta-\frac{\rho\sigma_xa}{\kappa}\right)c-\frac{\sigma_x^2c^2}{2\kappa^2}\right)t+\left(b-\frac{c}{\kappa}\right)\left(\left(\theta-\frac{\rho\sigma_xa}{\kappa}\right)-\frac{\sigma_x^2c}{\kappa^2}\right)\\&\quad\times\left(e^{\kappa t}-1\right)+\\&\quad-\frac{\sigma_x^2}{4\kappa}\left(b-\frac{c}{\kappa}\right)^2\left(e^{2\kappa t}-1\right)+\left(\lambda-\frac{1}{2}a^2\right)t-\lambda\int_0^t h\left(B(s)\right)\mathrm{d}s.\end{aligned}$$

Let $\alpha,\beta,\gamma\in\mathbb{R}$. The joint Laplace transform of the distribution of the random vector $\left(W_t^S,x_t,X_t\right)$ is going to be of the form

$$\begin{aligned}&\mathbb{E}\left[\exp\left(-\alpha W_T^S-\beta x_T-\gamma X_T\right)\middle|\mathcal{F}_t\right]\\&\quad=\exp\left(-A(t,T;\alpha,\beta,\gamma)W_t^S-B(t,T;\alpha,\beta,\gamma)x_t+C(t,T;\alpha,\beta,\gamma)\right).\end{aligned}$$

Setting $a=\alpha$ and $c=\gamma$, from the martingale property of $\exp\left(-aW_t^S-B(t)x_t-cX_t+D(t)\right)$ we have, for any $T\geq t\geq 0$

$$\begin{aligned}&\mathbb{E}\left[\exp\left(-\alpha W_T^S-B(T)x_T-\gamma X_T+D(T)\right)\middle|\mathcal{F}_t\right]\\&\quad=\exp\left(-\alpha W_t^S-B(t)x_t-\gamma X_t+D(t)\right).\end{aligned}$$

First of all, we impose $A(t,T;\alpha,\beta,\gamma):=\alpha$. Then, we set $B(T)=\beta$ and obtain

$$b=\left(\beta-\frac{\gamma}{\kappa}\right)e^{-\kappa T}+\frac{\gamma}{\kappa}$$

and

$$\begin{aligned}B(t)&=\left(b-\frac{\gamma}{\kappa}\right)e^{\kappa t}+\frac{\gamma}{\kappa}\\&=\left(\beta-\frac{\gamma}{\kappa}\right)e^{-\kappa(T-t)}+\frac{\gamma}{\kappa}.\end{aligned}$$

Setting

$$B(t,T;\alpha,\beta,\gamma):=\left(\beta-\frac{\gamma}{\kappa}\right)e^{-\kappa(T-t)}+\frac{\gamma}{\kappa},$$

we obtain

$$\begin{aligned}&\mathbb{E}\left[\exp\left(-\alpha W_T^S-\beta x_T-\gamma X_T+D(T)\right)\middle|\mathcal{F}_t\right]\\&\quad=\exp\left(-\alpha W_t^S-B(t,T;\alpha,\beta,\gamma)x_t-\gamma X_t+D(t)\right)\end{aligned}$$

and setting $C(t,T;\alpha,\beta,\gamma):=D(t)-D(T)$ we obtain the Laplace transform of interest, that reads

$$\begin{aligned}&\mathbb{E}\left[\exp\left(-\alpha W_T^S-\beta x_T-\gamma X_T\right)\middle|\mathcal{F}_t\right]\\&\quad=\exp\left(-\alpha W_t^S-B(t,T;\alpha,\beta,\gamma)x_t-\gamma X_t+C(t,T;\alpha,\beta,\gamma)\right).\end{aligned}$$

Standard computations deliver

$$\begin{aligned}C(t,T;\alpha,\beta,\gamma)&=\left(-\left(\theta-\frac{\rho\sigma_x\alpha}{\kappa}\right)\gamma+\frac{\sigma_x^2\gamma^2}{2\kappa^2}\right)(T-t)+\left(\beta-\frac{\gamma}{\kappa}\right)\\&\quad\times\left(\left(\theta-\frac{\rho\sigma_x\alpha}{\kappa}\right)-\frac{\sigma_x^2\gamma}{\kappa^2}\right)\left(e^{-\kappa(T-t)}-1\right)+\\&\quad-\frac{\sigma_x^2}{4\kappa}\left(\beta-\frac{\gamma}{\kappa}\right)^2\left(e^{-2\kappa(T-t)}-1\right)+\left(\frac{\alpha^2}{2}-\lambda\right)(T-t)\\&\quad+\lambda\int_t^T h\left(B(s)\right)\mathrm{d}s.\end{aligned}$$

and conclude the proof.

Proof of Corollary 5. Recalling (12), the futures price of interest reads

$$\begin{aligned}F(t,T)&=S_t\exp\left(\int_t^T r(s)\mathrm{d}s-\int_t^T g(s)\mathrm{d}s-\frac{\sigma_S^2}{2}(T-t)\right)\\&\quad\times\mathbb{E}\left[\exp\left(-\left(X_T-X_t\right)+\sigma_S\left(W_T^S-W_t^S\right)\right)\middle|\mathcal{F}_t\right].\end{aligned}$$

The expected value in the last expression can be computed using the Laplace transform derived in Proposition 4. Indeed, for $\beta=0$ we get

$$\begin{aligned}&\mathbb{E}\left[\exp\left(-\alpha W_T^S-\gamma X_T\right)\middle|\mathcal{F}_t\right]\\&\quad=\exp\Big[-\alpha W_t^S-\left(-\frac{\gamma}{\kappa}e^{-\kappa(T-t)}+\frac{\gamma}{\kappa}\right)x_t-\gamma X_t+\\&\quad+\left(-\left(\theta-\frac{\rho\sigma_x\alpha}{\kappa}\right)\gamma+\frac{\sigma_x^2\gamma^2}{2\kappa^2}\right)(T-t)-\frac{\gamma}{\kappa}\left(\left(\theta-\frac{\rho\sigma_x\alpha}{\kappa}\right)-\frac{\sigma_x^2\gamma}{\kappa^2}\right)\\&\quad\times\left(e^{-\kappa(T-t)}-1\right)+\\&\quad-\frac{\sigma_x^2}{4\kappa}\left(\frac{\gamma}{\kappa}\right)^2\left(e^{-2\kappa(T-t)}-1\right)+\left(\frac{\alpha^2}{2}-\lambda\right)(T-t)+\lambda\int_t^T h\left(B(s)\right)\mathrm{d}s\Big].\end{aligned}$$

Since both W_t^S and x_t are $\mathcal{F}_t$-measurable, rearranging the terms in the previous equality we get

$$\begin{aligned}&\mathbb{E}\left[\exp\left(-\alpha\left(W_T^S-W_t^S\right)-\gamma\left(X_T-X_t\right)\right)\middle|\mathcal{F}_t\right]\\&\quad=\exp\Big[\left(\frac{\gamma}{\kappa}e^{-\kappa(T-t)}-\frac{\gamma}{\kappa}\right)x_t\\&\quad+\left(-\left(\theta-\frac{\rho\sigma_x\alpha}{\kappa}\right)\gamma+\frac{\sigma_x^2\gamma^2}{2\kappa^2}\right)(T-t)-\frac{\gamma}{\kappa}\left(\left(\theta-\frac{\rho\sigma_x\alpha}{\kappa}\right)-\frac{\sigma_x^2\gamma}{\kappa^2}\right)\\&\quad\times\left(e^{-\kappa(T-t)}-1\right)+\\&\quad-\frac{\sigma_x^2}{4\kappa}\left(\frac{\gamma}{\kappa}\right)^2\left(e^{-2\kappa(T-t)}-1\right)+\left(\frac{\alpha^2}{2}-\lambda\right)(T-t)+\lambda\int_t^T h\left(B(s)\right)\mathrm{d}s\Big].\end{aligned}$$

Moving towards the expected value of interest in (12), we set $-\alpha=\sigma_S$, $\gamma=-1$ and get

$$\begin{aligned}&\mathbb{E}\left[\exp\left(\sigma_S\left(W_T^S-W_t^S\right)-\left(X_T-X_t\right)\right)\middle|\mathcal{F}_t\right]\\&=\exp\Big[\left(\frac{1}{\kappa}e^{-\kappa(T-t)}-\frac{1}{\kappa}\right)x_s\\&\quad+\left(-\left(\theta+\frac{\rho\sigma_x\sigma_S}{\kappa}\right)+\frac{\sigma_x^2}{2\kappa^2}\right)(T-t)-\frac{1}{\kappa}\left(\left(\theta+\frac{\rho\sigma_x\sigma_S}{\kappa}\right)-\frac{\sigma_x^2}{\kappa^2}\right)\\&\quad\times\left(e^{-\kappa(T-t)}-1\right)\\&\quad-\frac{\sigma_x^2}{4\kappa}\left(\frac{1}{\kappa}\right)^2\\&\quad\times\left(e^{-2\kappa(T-t)}-1\right)+\left(\frac{\sigma_S^2}{2}-\lambda\right)(T-t)+\lambda\int_t^T h\left(B(s)\right)\mathrm{d}s\Big].\end{aligned}$$

Setting $B(t,T):=\frac{1}{\kappa}\left(1-e^{-\kappa(T-t)}\right)$, rearranging the terms and using (15) for the integral of the jump component delivers the result.

Appendix C. Maximum likelihood estimation of the model

In order to retrieve an estimate of the parameters of the proposed model from a time series perspective, we start from the observed trajectories of S and $\hat{\delta}$ introduced in Section 2. Since the spot price S is actually proxied by the one-day ahead futures price while the convenience yield $\hat{\delta}$ is determined using the futures price with the

shortest maturity, we can assume that the trajectories of interest are directly observed under the equivalent martingale measure $\mathbb{Q}$.

Although the baseline model introduced in Section 3 does not include a jump component in the spot price process S, an extended version presented in Section 3.6 incorporates this feature by modifying the original SDE for S in (3) to the form given in (20). Consequently, we provide below a unified approximated maximum likelihood-based estimation of the full model, which also accounts for the jump component in S. Naturally, the estimates reported in Table 3 for the baseline model correspond to the case where no jumps are assumed in S, achieved by forcing the intensity λ^S of the associated jump process J^S to zero and neglecting the extra contribution to the variance of the increments of S in (28).

To estimate the parameters of the equations in (3)/(20)–(5), we use a simplified maximum likelihood estimation method. In particular, we discretize the model and maximize the likelihood of the innovation terms, specifically the Brownian increments and the jump components.[19] Although a more accurate but complex alternative is available (namely, the particle filtering algorithm, which extends the traditional Kalman filter to account for jumps, see Johannes et al. (2009) for details) we opt here for this simplified approach.

The Euler discretization[20] of the stochastic differential equations for S and x in (3)/(5) and (20) reads

$$\frac{S_{t+\Delta t}-S_t}{S_t} = \left(r(t)-\delta_t-\lambda^S m_J\right)\Delta t + \sigma_S \Delta W_t^S + \Delta J_t^S$$
$$x_{t+\Delta t}-x_{t^-} = \kappa\left(\theta - x_{t^-}\right)\Delta t + \sigma_x \Delta W_t^x + \Delta J_t$$

with $m_J = \mathbb{E}[Y]-1$ and that, using (10) to retrieve the dependence from δ_t, rewrites as

$$\frac{S_{t+\Delta t}-S_t}{S_t} - \left(r(t)-\delta_t-\lambda^S m_J\right)\Delta t = \sigma_S \Delta W_t^S + \Delta J_t^S$$
$$\delta_{t+\Delta t} - g(t+\Delta t) - \left(\delta_t - g(t)\right) - \kappa\left(\theta - \left(\delta_t - g(t)\right)\right)\Delta t = \sigma_x \Delta W_t^x + \Delta J_t. \tag{27}$$

Consider the random vector $\mathbf{Z}_t = \begin{bmatrix} Z_{1,t} & Z_{2,t}\end{bmatrix}'$ with

$$Z_{1,t} := \frac{S_{t+\Delta t}-S_t}{S_t} - \left(r(t)-\delta_t-\lambda^S m_J\right)\Delta t$$
$$Z_{2,t} := \delta_{t+\Delta t} - g(t+\Delta t) - \left(\delta_t - g(t)\right) - \kappa\left(\theta - \left(\delta_t - g(t)\right)\right)\Delta t.$$

Given the discrete time (daily) observations of S and $\hat{\delta}$ and a particular choice of the parameters $(\kappa, \theta, a, b, c, \lambda^S, \sigma_J)$, the realizations of $\mathbf{Z}$ can be explicitly computed.

We now aim to determine the theoretical distribution of $\mathbf{Z}$. As $\Delta t \approx 0$, we assume that between time t and $t+\Delta t$, at most one jump may affect S, δ, or both. Given the independence between the two jump components J_t^S and J_t, as well as between the Brownian shocks W_t^S and W_t^x, and assuming that the jumps in S and x are independent of each other and normally distributed with zero mean and variances σ_J^2 and ϕ^2, respectively, we obtain

$$\begin{bmatrix}\sigma_S \Delta W_t^S + \Delta J_t^S \\ \sigma_x \Delta W_t^x + \Delta J_t\end{bmatrix} \sim \mathcal{N}\left(\begin{bmatrix}0\\0\end{bmatrix}, \begin{bmatrix}\Delta t\sigma_S^2 + \sigma_J^2 & \Delta t\rho\sigma_S\sigma_x \\ \Delta t\rho\sigma_S\sigma_x & \Delta t\sigma_x^2 + \phi^2\end{bmatrix}\right) \tag{28}$$

if both processes experience a jump. If only one process is affected by a jump, or if no jumps occur between t and $t+\Delta t$, we simply remove the corresponding contribution from the main diagonal of the variance–covariance matrix in (28).

To determine whether a jump has occurred in any component of the random vector $\mathbf{Z}$, we introduce two new parameters, $\bar{\delta}$ and $\bar{S}$, which serve as jumping thresholds for the two processes. At any time step t, if $Z_{1,t}$ (respectively, $Z_{2,t}$) is smaller than $\bar{S}$ (respectively, $\bar{\delta}$), we assume that the observed shock is entirely due to W^S (respectively, W^x). Conversely, if $Z_{1,t}$ (respectively, $Z_{2,t}$) exceeds $\bar{S}$ (respectively, $\bar{\delta}$), we infer that the shock results from both W^S (respectively, W^x) and a jump.

Since the jumping thresholds $\bar{S}$ and $\bar{\delta}$ must be optimally determined, we include them as additional parameters in the model. Thus, the complete set of parameters to be estimated is given by $\Theta = (\sigma_S, \rho, \kappa, \theta, \sigma_x, a, b, c, \bar{\delta}, \phi, \bar{S}, \sigma_J)$. By explicitly incorporating the dependence on Θ and leveraging the independence of the innovation terms $\{\mathbf{Z}_t\}_t$, we derive the maximum likelihood estimator of Θ as

$$\hat{\Theta}^{MLE} = \underset{\Theta\in D}{\arg\max} \sum_t \ln f\left(\mathbf{Z}_t;\Theta\right) \tag{29}$$

where the density function f is given by (28) with a state-contingent variance–covariance matrix that depends on whether jumps are detected. The parameter space D is a twelve-dimensional domain[21] fo the parameters in Θ.

Finally, we obtain the estimate of the jump intensity λ as the annualized jumping frequency out of the resulting number of jumps counting how many times the second entry of the innovation terms $\{\mathbf{Z}_t\}_t$ (computed using $\hat{\Theta}^{MLE}$) exceeds the optimally determined $\bar{\delta}$.

Appendix D. Supplementary data

Supplementary material related to this article can be found online at https://doi.org/10.1016/j.eneco.2025.108586.

References

Almansour, A., 2016. Convenience yield in commodity price modelling: a regime switching approach. Energy Econ. 53, 238–247.

Benth, F.E., Piccirilli, M., Vargiolu, T., 2019. Mean-reverting additive energy forward curves in a heath-Jarrow-Morton framework. Math. Financ. Econ. 13 (1), 543–577.

Björk, T., Landen, C., 2000. On the Term Structure of Futures and Forward Prices. SSE/EFI Working Paper Series in Economics and Finance 0417, Stockholm School of Economics, URL https://EconPapers.repec.org/RePEc:hhs:hastef:0417.

Callegaro, G., Mazzoran, A., Sgarra, C., 2022. A self-exciting modeling framework for forward prices in power markets. Appl. Stoch. Models Bus. Ind. 38, 27–48.

Carmona, R., Ludkovski, M., 2004. Spot convenience yield models for the energy markets. Contemp. Math. 351, 65–80.

Casassus, J., Collin-Dufresne, P., 2005. Stochastic convenience yield implied from commodity futures and interest rates. J. Financ. 60 (5), 2283–2331.

Corsaro, S., Kyriakou, I., Marazzina, D., Marino, Z., 2019. A general framework for pricing Asian options under stochastic volatility on parallel architectures. European J. Oper. Res. 272 (3), 1082–1095.

Das, S., 2002. The surprise element: Jumps in interest rates. J. Econometrics 106 (1), 27–65.

Dingeç, K., Sak, H., Hörmann, W., 2015. Variance reduction for Asian options under a general model framework. Rev. Financ. 19 (2), 907–949.

Duffie, D., Pan, J., Singleton, K., 2000. Transform analysis and asset pricing for affine jump-diffusions. Econometrica 68 (6), 1343–1376.

Fang, F., Oosterlee, C.W., 2009. A novel pricing method for European options based on Fourier-cosine series expansions. SIAM J. Sci. Comput. 31 (2), 826–848.

Fusai, G., Kyriakou, I., 2016. General optimized lower and upper bounds for discrete and continuous arithmetic Asian options. Math. Oper. Res. 41 (2), 531–559.

Fusai, G., Meucci, A., 2008. Pricing discretely monitored Asian options under Lévy processes. J. Bank. Financ. 32 (10), 2076–2088.

García Mirantes, A., Población, J., Serna, G., 2013. The stochastic seasonal behavior of energy commodity convenience yields. Energy Econ. 40, 155–166.

Geman, H., Nguyen, V.N., 2005. Soybean inventory and forward curve dynamics. Manag. Sci. 51 (7), 1076–1091.

[19] For sake of computability, we assume here that also the jumps in x follow a normal distribution, whereas all of the other applications in the paper postulate a Laplace distribution for the jump component.

[20] As the Eqs. (3)/(20)–(5) admit a strong solution derived in Section 3.2, we could avoid the Euler discretization and evaluate numerically the transition densities (since, as highlighted in Remark 3, the distribution of x is not a standard one). However, since we are given daily observations, here $\Delta t \approx 0$ and the simplified approach we propose delivers reliable results as well.

[21] More precisely, in the numerical implementation we set $D = ([0.05, 4], [-1, 1], [0.05, 40], [-2, 2], [0.05, 4], [-12, 12], [5, 7], [-12, 12], [1, 4], [0.05, 4], [0.05, 4], [0.05, 4])$ and we repeat the optimization routine 50 times starting from different initial guesses drawn from a multivariate uniform distribution over D.

Gibson, R., Schwartz, E.S., 1990. Stochastic convenience yield and the pricing of oil contingent claims. J. Financ. 45 (3), 959–976.
Golyandina, N., Zhigljavsky, A., 2013. Singular Spectrum Analysis for time series. Springer.
Harvey, A.C., 1989. Forecasting, Structural Time Series Models and the Kalman Filter. Cambridge University Press.
Hilliard, J.E., Reis, J.A., 1999. Jump processes in commodity futures prices and options pricing. Am. J. Agric. Econ. 81 (2), 273–286.
Johannes, M.S., Polson, N.G., Stroud, J.R., 2009. Optimal filtering of jump diffusions: Extracting latent states from asset prices. Rev. Financ. Stud. 22 (7), 159–178.
Kou, S.G., Wang, H., 2004. Option pricing under a double exponential jump diffusion model. Manag. Sci. 50 (9), 1178–1192.
Kwiatkowski, D., Phillips, P.C.B., Schmidt, P., Shin, Y., 1992. Testing the null hypothesis of stationarity against the alternative of a unit root: How sure are we that economic time series have a unit root? J. Econometrics 54 (1), 159–178.
Kyriakou, I., Pouliasis, P.K., Papapostolou, N.C., 2016. Jumps and stochastic volatility in crude oil prices and advances in average option pricing. Quant. Finance 16 (12), 1859–1873.
Li, B., 2019. Pricing dynamics of natural gas futures. Energy Econ. 78, 91–108.
Lucia, J., Schwartz, E., 2002. Electricity prices and power derivatives: Evidence from the nordic power exchange. Rev. Deriv. Res. 5 (1), 5.
Merton, R.C., 1976. Option pricing when underlying stock returns are discontinuous. J. Financ. Econ. 3 (1), 125–144.
Miltersen, K.R., 2003. Commodity price modelling that matches current observables: a new approach. Quant. Finance 3 (1), 51–58.
Miltersen, K.R., Schwartz, E.S., 1998. Pricing of options on commodity futures with stochastic term structures of convenience yields and interest rates. J. Financ. Quant. Anal. 33 (1), 33–59.
Nguyen, D.B.B., Prokopczuk, M., 2019. Jumps in commodity markets. J. Commod. Mark. 13, 55–70.
Nicholas, K., 1939. Speculation and economic stability. Rev. Econ. Stud. 7 (1), 1–27.
Roncoroni, A., Fusai, G., Cummins, M., 2015. Handbook of Multi-Commodity Markets and Products: Structuring, Trading and Risk Management. Wiley.
Said, S.E., Dickey, D.A., 1984. Testing for unit roots in autoregressive-moving average models of unknown order. Biometrika 71 (3), 599–607.
Schönbucher, P.J., 2003. Credit Derivatives Pricing Models: Models, Pricing and Implementation. Wiley, Chichester, England.
Schwartz, E., Smith, J.E., 2000. Short-term variations and long-term dynamics in commodity prices. Manag. Sci. 46 (7), 893–911.
Svensson, L.E., 1994. Estimating and interpreting forward interest rates: Sweden 1992–1994. Cent. Econ. Policy Res. Discuss. Pap. No 1051.